Hierarchical scaling law for the strength of composite fibre bundles

CrossMark

Soraia Pimenta*, Silvestre T. Pinho

Department of Aeronautics, South Kensington Campus, Imperial College London. London SW7 2AZ, United Kingdom

ARTICLE INFO

ABSTRACT

This paper presents an analytical model for size effects on the longitudinal tensile strength of composite fibre bundles. The strength of individual fibres is modelled by a Weibull distribution, while the matrix (or fibre–matrix interface) is represented through a perfectly plastic shear-lag model. A probabilistic analysis of the failure process in hierarchical bundles (bundles of bundles) is performed, so that a scaling law relating the strength distributions and characteristic lengths of consecutive bundle levels is derived. An efficient numerical scheme (based on asymptotic limits) is proposed, hence coupon-sized bundle strength distributions are obtained almost instantaneously. Parametric studies show that both fibre and matrix properties are critical for bundle strength; model predictions at different scales are validated against experimental results available in the literature.

© 2013 Elsevier Ltd. All rights reserved.

1. Introduction

Size effects on the strength of composite materials are widely reported in the literature, but a universally accepted modelling strategy is still to be developed (Wisnom, 1999); this represents a significant challenge for the design of large structures. This paper presents a model for size effects on the longitudinal tensile strength of UniDirectional (UD) Fibre-Reinforced Polymers (FRPs), based on the stochastic variability of fibre strength and the definition of hierarchical fibre–matrix bundles.

Several theories have been proposed to model the relation between size and strength of structures. The stochastic approach, based on the Weakest Link Theory (WLT) and formalised by Weibull (1951), has been extensively applied to FRPs (Bažant and Pang, 2007; Wisnom, 1999). Deterministic size effects have also been studied by Bažant (1999, due to the energy dissipated by failure of quasi-brittle materials), Carpinteri (1994, due to the fractal self-similar failure of heterogeneous materials), and Wisnom et al. (2010, due to the change of failure mode in scaled laminated composites). All authors agree nevertheless that stochastic size effects are key for the strength of FRPs.

The WLT states that a chain withstands an external load only if all its elements survive the resulting stresses. Let $X_{\mathrm{U},\mathrm{r}}$ be the stochastic strength of the elements (with reference length l_{r}, all statistically identical and independent) under an uniform (subscript U) stress σ; the survival probability for each element is $S_{\mathrm{U},\mathrm{r}}(\sigma) = \Pr(X_{\mathrm{U},\mathrm{r}} > \sigma)$. Therefore, the survival probability of a chain (length $l_{\mathrm{n}} = n \cdot l_{\mathrm{r}}$) with n elements is

$$S_{\mathrm{U},\mathrm{n}}(\sigma) = [S_{\mathrm{U},\mathrm{r}}(\sigma)]^n \Rightarrow \ln\,[S_{\mathrm{U},\mathrm{n}}(\sigma)] = n \cdot \ln\,[S_{\mathrm{U},\mathrm{r}}(\sigma)] = \frac{l_{\mathrm{n}}}{l_{\mathrm{r}}} \cdot \ln\,[S_{\mathrm{U},\mathrm{r}}(\sigma)] \tag{1}$$

* Corresponding author. Tel.: +44 20 7594 5076; fax: +44 20 7594 5076.
E-mail address: soraia.pimenta@imperial.ac.uk (S. Pimenta).

Nomenclature

Uppercase variables

A	cross sectional area
C	perimeter
$\mathcal{C}_{\mathrm{K}}$	stress-concentrations strength parameter
CoV_X	coefficient of variation of strength
F	failure probability (strength distribution)
S	survival probability
V	volume fraction
X	longitudinal tensile strength

Lowercase variables

ϕ	diameter
i	bundle level
k	stress concentrations factor
l	length
m	Weibull shape parameter
n	number of elements/fibres
s	interfibre spacing
σ	longitudinal stress
τ	shear (yield) stress

Superscripts

f	fibre
[i]	bundle level
∞	remote

Subscripts

0	Weibull scale parameter
B	free edges boundary
c	control length
e	effective recovery length
K	linear stress concentrations state
L	pure linear stress state
M	matrix failure path
m	mean value
n	chain of elements
r	reference length/element
SL	shear-lag
U	uniform stress state

Weibull (1951) proposed a distribution for the strength of brittle materials, so that survival and failure probabilities of a chain under uniform stresses σ are

$$S_{\mathrm{U,n}}(\sigma) = \exp\left[-\frac{l_{\mathrm{n}}}{l_{\mathrm{r}}}\left(\frac{\sigma}{\sigma_0}\right)^m\right] \quad \text{and} \quad F_{\mathrm{U,n}}(\sigma) = 1-\exp\left[-\frac{l_{\mathrm{n}}}{l_{\mathrm{r}}}\left(\frac{\sigma}{\sigma_0}\right)^m\right] \tag{2}$$

where m and σ_0 are respectively the shape (size independent) and scale (measured at l_r) parameters of the distribution.

Eq. (2) has been widely used to model the length effect on the strength of technical fibres, e.g. glass or carbon (Curtin, 1999; Pradhan et al., 2010; Wisnom, 1999). While alternative strength distributions have been proposed (e.g. Beetz, 1982; Beyerlein and Phoenix, 1996a), Stoner et al. (1994) showed that a good agreement between Weibull's theory and experimental measurements can be achieved by taking the spurious effect of fibre gripping and testing variability into account.

At the FRP level, the parallel fibre arrangement and the presence of matrix result in a quasi-brittle failure. Beyerlein and Phoenix (1996a) and Kazanci (2004) tested micro-bundles (with 4 and 7 fibres respectively) and found that bundle strengths deviated significantly from Weibull distributions; moreover, some bundles (depending on the resin) had higher mean strength than the single-fibres, but considerably lower variability. At the macroscopic scale, Okabe and Takeda (2002) and Scott et al. (2011) observed several clusters of fibre breaks before final coupon failure. Wisnom (1999) also noted that both the magnitude of size effects and the variability of strength decrease for larger specimens. All these observations are incompatible with the WLT applied directly to the single-fibre level (Bažant, 1999; Wisnom, 1999).

The asymptotic behaviour of tensile strength of FRPs has been successfully modelled in the literature (see reviews from Bažant, 1999; Curtin, 1999; Wisnom, 1999). However, the recent developments in composites with thin plies (Sihn et al., 2007) and with discontinuous reinforcement — with individual fibres and bundles of various sizes (Harper et al., 2007; Pimenta et al., 2010) — requires developing and validating full scaling models. Wisnom (1999) suggests Fibre Bundle Models (FBMs, firstly developed by Daniels, 1945, and recently reviewed by Pradhan et al., 2010) have the potential to capture most of the physics involved in longitudinal tensile failure of FRPs and the associated size effects.

Several FBMs have been proposed to predict the longitudinal tensile strength and size effects in composites. The key challenge is to calculate the strength distribution of a bundle of parallel fibres with a given *characteristic length*, to then use the WLT (Eq. (1)) to scale the result for a chain of bundles (Curtin, 1991; Harlow and Phoenix, 1978a,b). Different fibre arrangements, matrix responses, load sharing schemes and magnitudes of stress concentrations have been assumed (see review from Curtin, 1999).

The complexity of most FBMs increases exponentially with the number of fibres considered, hence exact solutions are attainable for small bundles only; consequently, much work focused on asymptotic analyses (Curtin, 1993; Phoenix et al., 1997; Phoenix and Smith, 1983) and Monte-Carlo simulations (Landis et al., 2000; Mahesh et al., 2002; Okabe and Takeda, 2001; Wada and Fukuda, 1999). Most authors use a characteristic length independent of load and number of fibre breaks, although this is known not to be correct (Behzadi et al., 2009; Phoenix et al., 1988).

Laffan et al. (2010) and Pimenta et al. (2010) reported self-similar or quasi-fractal fracture surfaces in thin (under 0.5 mm) UD laminas and fibre bundles; this provides experimental evidence that the length-scale of the failure process increases with the number of fibres involved. Moreover, such observations suggest a hierarchical failure process, hence supporting the use of hierarchical models — e.g. Newman and Gabrielov's (1991) model for *dry* bundles. Here, considering that a bundle of level [i+1] is composed of two sub-bundles of level [i], strength distributions were calculated recursively as

$$F^{[i+1]}(\sigma) = F^{[i]}(\sigma) \cdot [2 \cdot F^{[i]}(2 \cdot \sigma) - F^{[i]}(\sigma)] \tag{3}$$

where $F^{[i]}(\sigma)$ is the failure probability of a level-[i] bundle under an applied stress σ. The recursive nature of this scaling law also allowed its efficient implementation, so that large-scale bundles could be computed. However — being a model for dry bundles — it does not consider the effect of an embedding matrix, and does not include any characteristic length (which is paramount for quasi-brittle materials, Bažant, 1999); the model is also inconsistent with the WLT for length scaling.

Altogether, a comprehensive explanation of the micromechanics and statistics of tensile failure in composites is yet to be provided, as are validated quantitative predictions over a complete range of scales. Still, FBMs surface as one of the most promising approaches to overcome this knowledge gap.

This paper presents the development, implementation and validation of a FBM for predicting size effects on the longitudinal tensile strength of composite bundles. Following Newman and Gabrielov's (1991) work, bundles are hierarchically organised; however, the role of the matrix (or fibre–matrix interface) is now considered through a simplified shear-lag model, in which the characteristic length scales hierarchically as well.

This paper is organised as follows: Section 2 presents the analytical model for predicting strength distributions of FRP bundles of different dimensions. Section 3 explores modelling results (including experimental validation), subsequently discussed in Section 4. Finally, Section 5 draws the main conclusions.

2. Model development

2.1. Fibre bundle geometry and shear-lag boundary

This model is based on hierarchical fibre–matrix bundles (Fig. 1a). These are generated by pairing individual fibres (level-[0]) into level-[1] bundles, and then sequentially grouping two level-[i] bundles into one level-[i+1] bundle (Newman and Gabrielov, 1991). The number of fibres ($n^{[i]}$) in a level-[i] bundle is therefore:

$$n^{[i]} = 2^i \Leftrightarrow i = \log_2 n^{[i]} \tag{4}$$

The fibres (superscript f, diameter ϕ^f, circumference C^f and area A^f) are embedded in the matrix (with volume fraction V^f) in a square architecture (Fig. 1b).

During hierarchical failure of a large composite bundle (Fig. 2a), shear-lag stresses will be transferred between the (unbroken) surrounding material and a broken level-[i] bundle through the *shear-lag boundary*, with perimeter $C^{[i]}$. Considering preferential interfacial debonding (Fig. 2b),

$$C^{[i]} = 3 \cdot C^f + 4 \cdot \left[(\sqrt{n^{[i]}} - 1) \cdot s_Q + (\sqrt{n^{[i]}} - 2) \cdot \frac{C^f}{2} \right] \quad \text{with } s_Q = \left(\frac{\sqrt{\pi}}{2 \cdot \sqrt{V^f}} - 1 \right) \cdot \phi^f \tag{5}$$

This expression is strictly valid only for even values of *i*, but used for any bundle size so that $C^{[i]}$ is a smooth function of $n^{[i]}$.

Other geometries for bundles and their boundaries (e.g. hexagonal fibre arrangement with fractal boundary, preferential matrix failure, free-edge effects) are considered in Appendix A. These variations are shown to have a minor influence on calculated bundle strength distributions (as already suggested by Curtin and Takeda, 1998).

2.2. Stress field around a fibre break and definition of the control region

Consider a level-[1] bundle of reference length l_r, composed of two level-[0] fibres ($\mathcal{A}$ and $\mathcal{B}$) in a soft matrix (i=1 in Fig. 1a). The bundle is loaded in tension by a progressively increasing remote stress σ^∞, so that each fibre undergoes
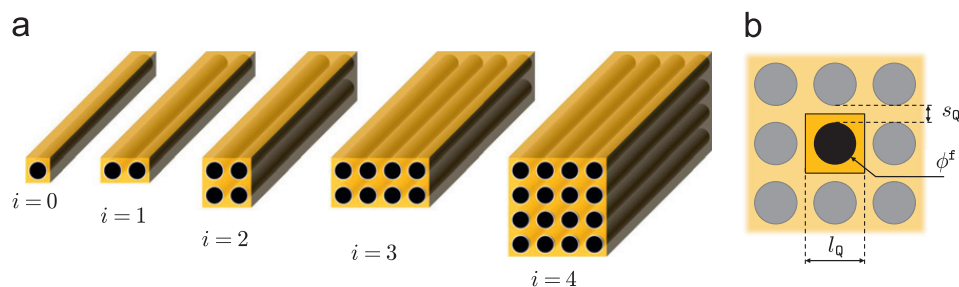

Fig. 1. Hierarchical bundles in square fibre arrangement. (a) Bundle hierarchy. (b) Fibre arrangement.
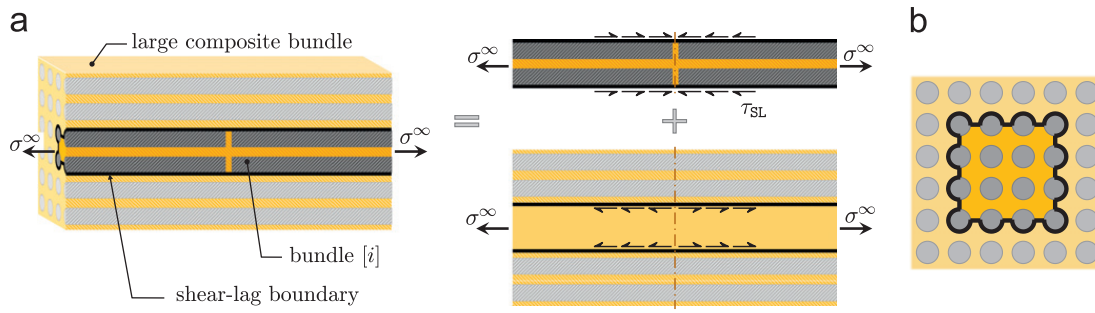
Fig. 2. Shear-lag boundary (assuming preferential interfacial failure). (a) Longitudinal view. (b) Section view.
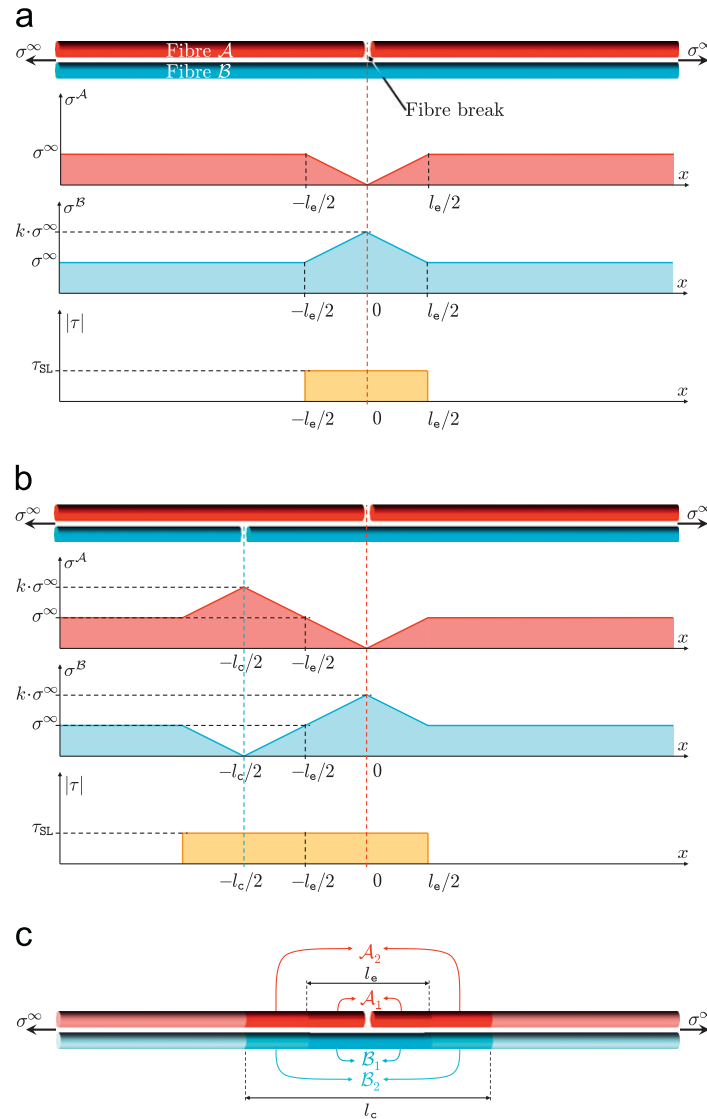
Fig. 3. Stress fields and length scales in a level-[1] fibre bundle. (a) Stress fields after first fibre failure. (b) Definition of critical distance between fibre breaks: the bundle fails only if fibre $\mathcal{B}$ breaks at a distance smaller than $l_c/2$ from the break in fibre $\mathcal{A}$. (c) Definition of the control region and fibre segments.

a uniform stress state $\sigma^{\mathcal{A}} = \sigma^{\mathcal{B}} = \sigma^{\infty}$. Note that longitudinal stresses are expressed as fibre stresses, i.e. normalised by the area of fibres in the cross section.

Assume that fibre $\mathcal{A}$ fails at the location $x=0$ under a given σ^{∞} (Fig. 3a). Shear-lag models have been shown to accurately reproduce the resulting stress fields, as validated by more complex Finite Element analyses (Landis and McMeeking, 1999; de Morais, 2001). The in situ response of the matrix/interface to this event is complex, as for instance epoxy is usually brittle in bulk, but actually ductile and much stronger in situ (Gulino et al., 1991; Hobbiebrunken et al.,

2007; de Morais, 2001). This, together with the lack of agreement in the literature on whether fibre failure should be modelled through energy or stress based approaches (Nairn, 1997; Zhandarov et al., 1998), supports the use of a perfectly plastic shear-lag approach, for the sake of simplicity (Landis and McMeeking, 1999; de Morais, 2006).

According to perfectly plastic shear-lag, the failed fibre $\mathcal{A}$ recovers the remote stress σ^∞ within the level-[0] *effective recovery length* (subscript $_e$), defined as (Kelly and Tyson, 1965)

$$l_e^{[0]}(\sigma^\infty) = 2 \cdot \frac{A^f}{C^{[0]} \cdot \tau_{SL}} \cdot \sigma^\infty \tag{6}$$

Here, τ_{SL} is the matrix/interface yield stress, and $C^{[0]}$ is the perimeter of the level-[0] shear-lag boundary (Eq. (5) implies $C^{[0]} = C^f$).

Conversely, fibre $\mathcal{B}$ undergoes linear stress concentrations within the length $l_e^{[0]}$ (Fig. 3a). In this model, equilibrium of the 2 fibres yields a stress concentration factor $k=2$. However, the true value of k near a cluster of fibre breaks is still an open issue, and depends on local fibre arrangement, size of broken cluster, matrix response and dynamic effects (Accorsi et al., 1996; Beyerlein and Phoenix, 1996b; Hedgepeth, 1961; Mahesh et al., 2002; de Morais, 2001; Nedele and Wisnom, 1994; Swolfs et al., 2013). Therefore, k will be treated as free parameter.

Bundle failure requires that both fibres $\mathcal{A}$ and $\mathcal{B}$ break in nearby locations, so as to promote complete yielding of matrix/interface between breaks (Fig. 3b). Therefore, once fibre $\mathcal{A}$ fails, the level-[1] *control region* (subscript $_c$) — within which a break in fibre $\mathcal{B}$ leads to bundle failure — has a length defined by

$$l_c^{[1]}(\sigma^\infty) = 2 \cdot l_e^{[0]}(\sigma^\infty) = 4 \cdot \frac{A^f}{C^{[0]} \cdot \tau_{SL}} \cdot \sigma^\infty \tag{7}$$

This region, centred at the first fibre break, is partitioned into 4 *fibre segments* ($\mathcal{A}_1$, $\mathcal{A}_2$, $\mathcal{B}_1$ and $\mathcal{B}_2$) of equal length $l_e^{[0]}$ (Fig. 3c). The probability of failure of the level-[1] bundle within the *control length* will be determined in Section 2.3.

This definition of $l_c^{[1]}$ differs from other characteristic lengths in the literature. Firstly, $l_c^{[1]} \propto \sigma^\infty$ (as opposed to fixing $l_c^{[1]}$ at a characteristic stress, as done by Curtis, 1986; Fukuda and Kawata, 1977; Harlow and Phoenix, 1978a; Okabe and Takeda, 2001). Secondly, $l_c^{[1]} = 2 \cdot l_e^{[0]}$; while Curtin (1993) and Phoenix et al. (1997) proposed $l_c^{[1]} \le l_e^{[0]}$ for global load sharing, Eq. (7) defines the shortest statistically independent partition of a level-[1] bundle. Finally, the control length of a larger level-[i+1] bundle will be scaled hierarchically in Section 2.4.

2.3. Statistical analysis of level-[1] bundle failure

The strength distribution of the level-[1] bundle analysed in Fig. 3 will be determined under the following assumptions:

A(i) At each remote stress σ^∞, the bundle is represented by a chain of independent control regions of length $l_c^{[1]}$ (Eq. (7)). This shifts the first fibre break to the centre, thus neglecting bundle-end effects.

A(ii) Within a control region, each fibre may break only once (equivalent to the WLT); this guarantees that the stress fields presented in Fig. 3 are always valid.

Statistically, a *level-[1] bundle survives* the remote stress σ^∞ in the control length *if* (i) all its *4 fibre segments survive the uniform stress σ^∞*, or (ii) *the weakest fibre fails under σ^∞ and the strongest fibre survives the resulting stress field* — comprising one segment under the uniform stress σ^∞, and another segment under linear stress concentrations (factor k). The survival probability of the level-[1] bundle under uniform (subscript $_U$) stresses σ^∞ within the control length is then:

$$S_{U,c}^{[1]}(\sigma^\infty) = S_{U,e}^{[0]}(\sigma^\infty)^4 + 2 \cdot [1 - S_{U,e}^{[0]}(\sigma^\infty)^2] \cdot S_{U,e}^{[0]}(\sigma^\infty) \cdot S_{K,e}^{[0]}(\sigma^\infty) \tag{8}$$

where:

- $S_{U,e}^{[0]}(\sigma^\infty)$ is the survival probability of a single-fibre segment loaded by a uniform stress σ^∞ within the length $l_e^{[0]}$. Assuming that fibre strength follows a Weibull distribution with survival probability $S_{U,r}^{[0]}$ at the reference length l_r (with parameters m and σ_0^f as shown below), then WLT scaling (Eq. (2)) implies

$$S_{U,r}^{[0]} = \exp\left[-\left(\frac{\sigma^\infty}{\sigma_0^f}\right)^m\right] \quad \text{and} \quad S_{U,e}^{[0]} = \exp\left[-\frac{l_e^{[0]}}{l_r} \cdot \left(\frac{\sigma^\infty}{\sigma_0^f}\right)^m\right] \tag{9}$$

- $S_{K,e}^{[0]}(\sigma^\infty)$ is the survival probability of a single-fibre segment loaded under linear stress concentrations (variable remote stress σ^∞ and constant factor k) within the length $l_e^{[0]}$. Generalising the WLT to non-uniform chain stresses (Appendix B),

$$S_{K,e}^{[0]} = \exp\left[-\mathcal{C}_K \cdot \frac{l_e^{[0]}}{l_r} \cdot \left(\frac{\sigma^\infty}{\sigma_0^f}\right)^m\right] \quad \text{where } \mathcal{C}_K = \frac{k^{m+1}-1}{(m+1) \cdot (k-1)} \tag{10}$$

While the level-[1] scaling law in Eq. (8) was derived from a purely statistical argument, Appendix C shows it actually corresponds to the following physical sequences of events leading to bundle failure:

E_1: failure of the weakest fibre and immediate (unstable) failure (with no increment of σ^∞) of segment $\mathcal{B}_1$ due to stress concentrations;

E_2: failure of the weakest fibre and later (after incrementing σ^∞) failure of the stress concentrations segment $\mathcal{B}_1$;

E_3: failure of the weakest fibre and later failure of the far-segment $\mathcal{B}_2$ (*stable* failure due to independent fibre flaws). This includes bundle failure by growth and coalescence of matrix damage between two previously formed breaks.

2.4. Hierarchical law for bundle failure

Eq. (8) relates the strength distribution of a single fibre to that of a level-[1] bundle. Assuming a self-similar hierarchical failure process as reported by Laffan et al. (2010) and Pimenta et al. (2010), this can be extrapolated to any bundle level and used recursively throughout bundle hierarchy. Consequently, the survival probability of a level-[$i+1$] bundle under uniform stresses is (omitting σ^∞ for readability)

$$S_{U,c}^{[i+1]} = (S_{U,e}^{[i]})^4 + 2 \cdot [1-(S_{U,e}^{[i]})^2] \cdot S_{U,e}^{[i]} \cdot S_{K,e}^{[i]} \tag{11}$$

Level-[i] survival probabilities on the right-hand side are defined at the respective effective recovery length $l_e^{[i]}(\sigma^\infty)$, while $S_{U,c}^{[i+1]}$ is defined at the level-[$i+1$] control length. Contrary to most fibre bundle models in the literature (Curtin, 1991; Curtis, 1986; Fukuda and Kawata, 1977; Harlow and Phoenix, 1978a; Okabe and Takeda, 2001), these characteristic lengths are also scaled hierarchically from their original definition. Using the shear-lag perimeters defined in Eq. (5):

$$l_e^{[i]}(\sigma^\infty) \overset{\text{Eq. (6)}}{=} 2 \cdot \frac{n^{[i]} \cdot A^{\mathrm{f}}}{C^{[i]} \cdot \tau_{\mathrm{SL}}} \cdot \sigma^\infty, \quad l_c^{[i+1]}(\sigma^\infty) \overset{\text{Eq. (7)}}{=} 2 \cdot l_e^{[i]}(\sigma^\infty) \tag{12}$$

Eq. (11) can be written in both the following logarithmic forms:

$$\ln(S_{U,c}^{[i+1]}) = 4 \cdot \ln(S_{U,e}^{[i]}) + \ln\left(1 + 2 \cdot \frac{S_{K,e}^{[i]}}{(S_{U,e}^{[i]})^3} - 2 \cdot \frac{S_{K,e}^{[i]}}{S_{U,e}^{[i]}}\right)$$

$$= \ln(S_{U,e}^{[i]}) + \ln(S_{K,e}^{[i]}) + \ln\left(2 + \frac{(S_{U,e}^{[i]})^3}{S_{K,e}^{[i]}} - 2 \cdot (S_{U,e}^{[i]})^2\right) \tag{13}$$

Scaling to the reference length (using the WLT in Eq. (1) and $l_c^{[i+1]}$ in Eq. (12)),

$$\ln(S_{U,r}^{[i+1]}) = 2 \cdot \ln(S_{U,r}^{[i]}) + \frac{l_r}{2 \cdot l_e^{[i]}} \cdot \ln\left(1 + 2 \cdot \left[\frac{S_{K,r}^{[i]}}{(S_{U,r}^{[i]})^3}\right]^{l_e^{[i]}/l_r} - 2\left[\frac{S_{K,r}^{[i]}}{S_{U,r}^{[i]}}\right]^{l_e^{[i]}/l_r}\right)$$

$$= \frac{\ln(S_{U,r}^{[i]}) + \ln(S_{K,r}^{[i]})}{2} + \frac{l_r}{2 \cdot l_e^{[i]}} \cdot \ln\left(2 + \left[\frac{(S_{U,r}^{[i]})^3}{S_{K,r}^{[i]}}\right]^{l_e^{[i]}/l_r} - 2 \cdot [(S_{U,r}^{[i]})^2]^{l_e^{[i]}/l_r}\right) \tag{14}$$

The expressions above are analytically equivalent but prone to different numerical errors (due to exponential arguments); consequently, both forms will be used (Section 2.6).

The level-[i] survival probability under linear stress concentrations $S_{K,r}^{[i]}(\sigma^\infty)$ can be calculated from $S_{U,r}^{[i]}(\sigma^\infty)$. Bundle strengths do not follow Weibull distributions when $i > 0$, hence the generic relation derived in Appendix B must be employed:

$$\ln[S_{K,r}^{[i]}(\sigma^\infty)] = \begin{cases} \dfrac{k \cdot \ln[S_{L,r}^{[i]}(k \cdot \sigma^\infty)] - \ln[S_{L,r}^{[i]}(\sigma^\infty)]}{k-1} & \text{if } k > 1 \\ \ln[S_{U,r}^{[i]}(\sigma^\infty)] & \text{if } k = 1 \end{cases} \quad \text{where } \ln[S_{L,r}^{[i]}(\sigma)] = \frac{1}{\sigma}\int_{\sigma_L = 0}^{\sigma} \ln[S_{U,r}^{[i]}(\sigma_L)] \, d\sigma_L \tag{15}$$

2.5. Asymptotic behaviour

If fibre strength follows a Weibull distribution (Eq. (9)), then each tail of any bundle strength distributions tends asymptotically to a Weibull as well (Appendix D):

- The Right Tail Asymptote (RTA, $\sigma^\infty \to \infty$) of a bundle survival probability is

$$S_{U,r,\text{RTA}}^{[i]}(\sigma^\infty) = \exp\left[-\left(\frac{\sigma^\infty}{\sigma_{0,\text{RTA}}^{[i]}}\right)^m\right] \quad \text{with } \sigma_{0,\text{RTA}}^{[i]} = \begin{cases} 2^{-i/m} \cdot \sigma_0^{\mathrm{f}} & \text{if } \mathcal{C}_K \geq 3 \\ \left(\dfrac{1+\mathcal{C}_K}{2}\right)^{-i/m} \cdot \sigma_0^{\mathrm{f}} & \text{if } \mathcal{C}_K < 3 \end{cases} \tag{16}$$

This preserves the single-fibre shape parameter m. As most technical fibres (e.g. carbon and glass) have $\mathcal{C}_K \geq 3$ ($m \gtrsim 2.6$ with $k=2$ in Eq. (10)), the RTA of a bundle strength distribution corresponds to the WLT applied to the fibre level. This has been observed in other FBMs as well (Harlow and Phoenix, 1978b).

- The Left Tail Asymptote (LTA, $\sigma^\infty \to 0$) of a bundle survival probability is defined recursively as

$$S_{U,r,LTA}^{[i+1]}(\sigma^\infty) = \exp\left[-4 \cdot \mathcal{C}_{K,LTA}^{[i]} \cdot \frac{n^{[i]} \cdot A^f \cdot \sigma_{0,LTA}^{[i]}}{C^{[i]} \cdot \tau_{SL} \cdot l_r} \cdot \left(\frac{\sigma^\infty}{\sigma_{0,LTA}^{[i]}}\right)^{2 \cdot m_{LTA}^{[i]} + 1}\right] \qquad (17)$$

Level-[i] parameters are defined in Eq. (D.8). It should be noticed that the shape parameter of LTAs more than doubles with each hierarchical level; therefore, one can expect lower variability for the strength of larger bundles.
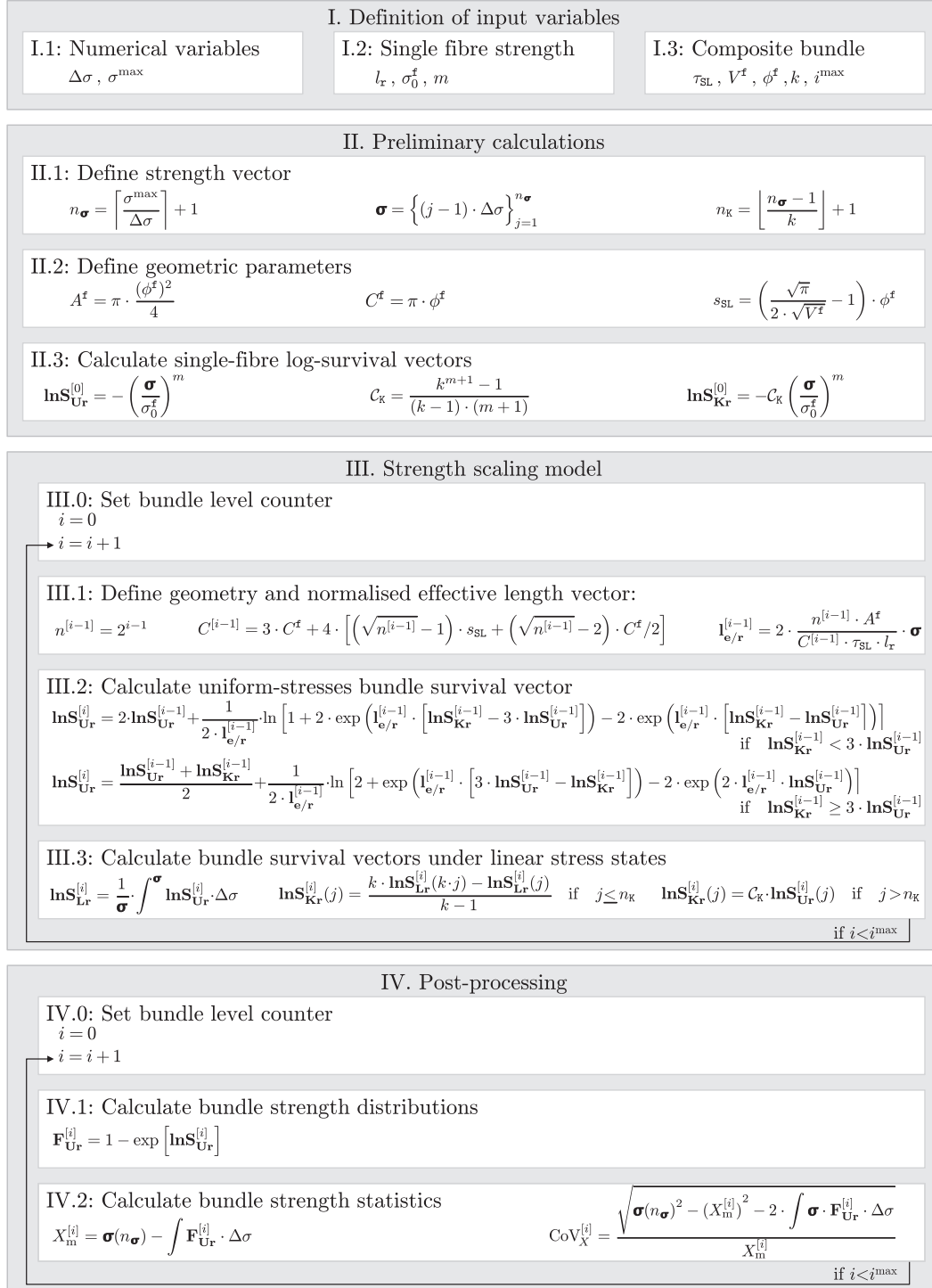

I. Definition of input variables

I.1: Numerical variables	I.2: Single fibre strength	I.3: Composite bundle
$\Delta\sigma$, σ^{max}	l_r , σ_0^f , m	τ_{SL} , V^f , ϕ^f , k , i^{max}

II. Preliminary calculations

II.1: Define strength vector

$$n_{\boldsymbol{\sigma}} = \left\lceil \frac{\sigma^{max}}{\Delta\sigma} \right\rceil + 1 \qquad\qquad \boldsymbol{\sigma} = \left\{(j-1)\cdot\Delta\sigma\right\}_{j=1}^{n_{\boldsymbol{\sigma}}} \qquad\qquad n_K = \left\lfloor \frac{n_{\boldsymbol{\sigma}} - 1}{k} \right\rfloor + 1$$

II.2: Define geometric parameters

$$A^f = \pi \cdot \frac{(\phi^f)^2}{4} \qquad\qquad C^f = \pi \cdot \phi^f \qquad\qquad s_{SL} = \left(\frac{\sqrt{\pi}}{2\cdot\sqrt{V^f}} - 1\right)\cdot\phi^f$$

II.3: Calculate single-fibre log-survival vectors

$$\ln S_{Ur}^{[0]} = -\left(\frac{\boldsymbol{\sigma}}{\sigma_0^f}\right)^m \qquad\qquad \mathcal{C}_K = \frac{k^{m+1} - 1}{(k-1)\cdot(m+1)} \qquad\qquad \ln S_{Kr}^{[0]} = -\mathcal{C}_K\left(\frac{\boldsymbol{\sigma}}{\sigma_0^f}\right)^m$$

III. Strength scaling model

III.0: Set bundle level counter
$i = 0$
→ $i = i + 1$

III.1: Define geometry and normalised effective length vector:

$$n^{[i-1]} = 2^{i-1} \qquad C^{[i-1]} = 3\cdot C^f + 4\cdot\left[\left(\sqrt{n^{[i-1]}} - 1\right)\cdot s_{SL} + \left(\sqrt{n^{[i-1]}} - 2\right)\cdot C^f/2\right] \qquad l_{e/r}^{[i-1]} = 2\cdot\frac{n^{[i-1]}\cdot A^f}{C^{[i-1]}\cdot\tau_{SL}\cdot l_r}\cdot\boldsymbol{\sigma}$$

III.2: Calculate uniform-stresses bundle survival vector

$$\ln S_{Ur}^{[i]} = 2\cdot\ln S_{Ur}^{[i-1]} + \frac{1}{2\cdot l_{e/r}^{[i-1]}}\cdot\ln\left[1 + 2\cdot\exp\left(l_{e/r}^{[i-1]}\cdot\left[\ln S_{Kr}^{[i-1]} - 3\cdot\ln S_{Ur}^{[i-1]}\right]\right) - 2\cdot\exp\left(l_{e/r}^{[i-1]}\cdot\left[\ln S_{Kr}^{[i-1]} - \ln S_{Ur}^{[i-1]}\right]\right)\right]$$
$$\text{if}\quad \ln S_{Kr}^{[i-1]} < 3\cdot\ln S_{Ur}^{[i-1]}$$

$$\ln S_{Ur}^{[i]} = \frac{\ln S_{Ur}^{[i-1]} + \ln S_{Kr}^{[i-1]}}{2} + \frac{1}{2\cdot l_{e/r}^{[i-1]}}\cdot\ln\left[2 + \exp\left(l_{e/r}^{[i-1]}\cdot\left[3\cdot\ln S_{Ur}^{[i-1]} - \ln S_{Kr}^{[i-1]}\right]\right) - 2\cdot\exp\left(2\cdot l_{e/r}^{[i-1]}\cdot\ln S_{Ur}^{[i-1]}\right)\right]$$
$$\text{if}\quad \ln S_{Kr}^{[i-1]} \geq 3\cdot\ln S_{Ur}^{[i-1]}$$

III.3: Calculate bundle survival vectors under linear stress states

$$\ln S_{Lr}^{[i]} = \frac{1}{\boldsymbol{\sigma}}\int^{\boldsymbol{\sigma}}\ln S_{Ur}^{[i]}\cdot\Delta\sigma \qquad \ln S_{Kr}^{[i]}(j) = \frac{k\cdot\ln S_{Lr}^{[i]}(k\cdot j) - \ln S_{Lr}^{[i]}(j)}{k-1} \quad \text{if}\quad j \leq n_K \qquad \ln S_{Kr}^{[i]}(j) = \mathcal{C}_K\cdot\ln S_{Ur}^{[i]}(j) \quad \text{if}\quad j > n_K$$

$$\text{if}\ i < i^{max}$$

IV. Post-processing

IV.0: Set bundle level counter
$i = 0$
→ $i = i + 1$

IV.1: Calculate bundle strength distributions

$$\mathbf{F}_{Ur}^{[i]} = 1 - \exp\left[\ln S_{Ur}^{[i]}\right]$$

IV.2: Calculate bundle strength statistics

$$X_m^{[i]} = \boldsymbol{\sigma}(n_{\boldsymbol{\sigma}}) - \int \mathbf{F}_{Ur}^{[i]}\cdot\Delta\sigma \qquad\qquad \text{CoV}_X^{[i]} = \frac{\sqrt{\boldsymbol{\sigma}(n_{\boldsymbol{\sigma}})^2 - \left(X_m^{[i]}\right)^2 - 2\cdot\int\boldsymbol{\sigma}\cdot\mathbf{F}_{Ur}^{[i]}\cdot\Delta\sigma}}{X_m^{[i]}}$$

$$\text{if}\ i < i^{max}$$

Fig. 4. Numerical implementation.

Such behaviour is typical of FBMs (Harlow and Phoenix, 1978b), although m_{LTA} here increases in a more pronounced way (due to $l_c^{[i+1]} \propto \sigma^\infty$).

In addition to providing further insight on bundle strength distributions and size effects, the RTA behaviour is key for the implementation of this model (Section 2.6). Eqs. (14) and (15) show that defining $S_{U,r}^{[i+1]}(\sigma^\infty)$ requires calculating $S_{U,r}^{[i]}(k \cdot \sigma^\infty)$, and thus (following a recursive procedure down to the single-fibre level) calculating $S_{U,r}^{[0]}(k^{i+1} \cdot \sigma^\infty)$. This becomes intractable as bundle level increases. Fortunately, the Weibull-like behaviour of RTAs (Eq. (16)) allows replacing the general relation between $S_{U,r}^{[i]}(\sigma^\infty)$ and $S_{K,r}^{[i]}(\sigma^\infty)$ (Eq. (15)) with its closed-form result for Weibull distributions (Eq. (B.7)), when $\sigma^\infty \to \infty$:

$$\lim_{\sigma^\infty \to \infty} \ln [S_{K,r}^{[i]}(\sigma^\infty)] = \mathcal{C}_K \cdot \ln [S_{U,r}^{[i]}(\sigma^\infty)], \quad \forall i \geq 0 \tag{18}$$

This eliminates the need to compute $S_{U,r}^{[i]}(k \cdot \sigma^\infty)$ for large values of σ^∞.

2.6. Numerical implementation

An overview of the numerical implementation of the present model is shown in Fig. 4; using array programming (e.g. MATLAB) greatly simplifies the implementation and reduces running time, hence the following remarks are of relevance:

- In the numerical implementation, the remote stress σ^∞ becomes a discrete vector $\boldsymbol{\sigma}$, with n_σ evenly spaced stress values from $\sigma^\infty = 0$ to $\sigma^\infty \geq \sigma^{max}$ (step size $\Delta\sigma$).
- Accordingly, most variables are expressed in vectorial form (indicated in upright bold in Fig. 4); all arithmetic operators represent pointwise calculations. Survival distributions are stored in logarithmic form, $\mathbf{lnS} \equiv \{\ln[S(\sigma^\infty)]\}$.
- Integration symbols represent numerical integration; these can be efficiently evaluated using MATLAB's in-built `trapz` and `cumtrapz` functions.
- Module IV calculates bundle strength distributions $F_{U,r}^{[i]}(\sigma) = \Pr(X_{U,r}^{[i]} \leq \sigma)$, where $X_{U,r}^{[i]}$ is the stochastic strength of a level-[i] bundle of length l_r under uniform stresses. Mean values ($X_m^{[i]}$) and Coefficients of Variation (CoV$_X^{[i]}$) depend directly on the cumulative distribution function, as a result of integration by parts.

3. Results

3.1. Analysis of model predictions

Fig. 5 summarises the results of the model for nominal input parameters (Table 1). Predicted bundle strength distributions (Fig. 5a) evidence size effects, with larger bundles (e.g. $i=15$) being weaker but less variable than their constituent fibres ($i=0$).

In Fig. 5b, the model predicts an initial strengthening throughout bundle hierarchy and steep reduction in variability (validated experimentally in Fig. 12); these aspects differ from Newman and Gabrielov's (1991) model.

The Weibull plot in Fig. 5c shows a concave-down curvature for all $i > 0$; this curvature initially increases for small bundles, but is progressively reduced for larger bundles within a 0.01−99.99% probability range. Fig. 5d highlights the asymptotic behaviour of bundle strength distributions (Eqs. (17) for LTAs and (16) for RTAs); as bundle level increases, these asymptotes are valid for progressively more reduced tails. Such behaviour is common to other FBMs (Harlow and Phoenix, 1978b).

3.2. Convergence study

The numerical implementation of the model (Section 2.6) is validated in Fig. 6, by studying the convergence of the CoV of strength distributions (sensitive to both mean value and tails) when $\Delta\sigma \to 0$ and $\sigma^{max} \to \infty$. The effect of using RTAs (Eq. (18)) in the formulation is noticeable in Fig. 6b: the asymptotic relation is activated for $\sigma^\infty > \sigma^{max}/k$, thus resulting in very large errors when σ^{max} is too small for the asymptote to be applicable. Nevertheless, a fully converged set of strength distributions (from the single fibre to a standard coupon-size FRP) is computed in less than a second.

3.3. Parametric study on fibre and matrix properties

The relation between single-fibre and bundle strength statistics is shown in Figs. 7 and 8. Mean bundle strengths increase as fibres become stronger (Fig. 7), with a directly proportional relation for constant fibre-to-matrix strength ratios. Fig. 8 shows that, for a deterministic fibre strength, the model predicts no size effects; for a small CoV$_X^f$ the model converges to the WLT (Eq. (16)), albeit at a slower rate for large bundles.
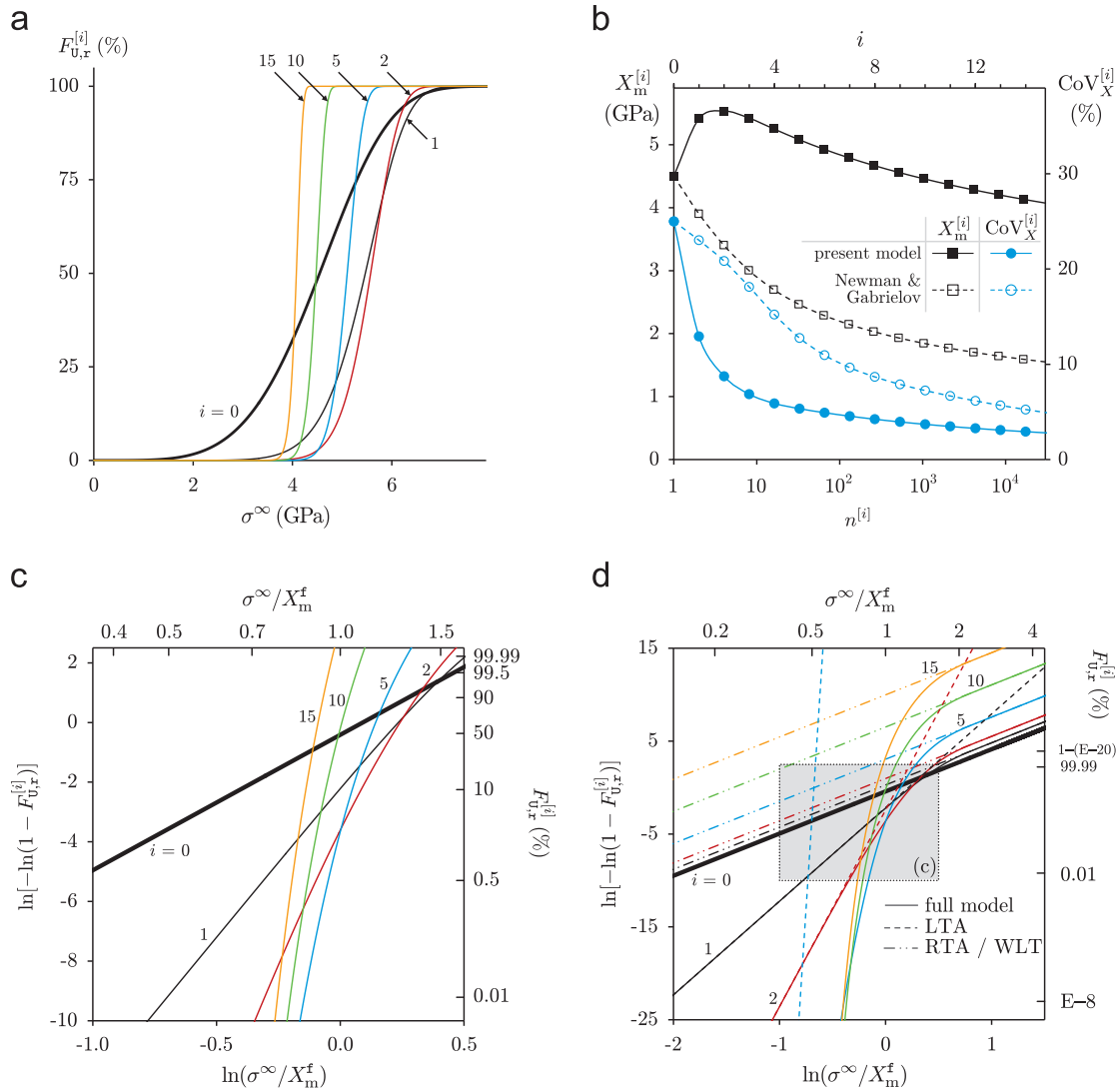
Fig. 5. Overview of model results. (a) Predicted bundle strength distributions (for several levels i). (b) Bundle strength size effect: present model vs. Newman and Gabrielov (1991). (c) Weibull plot for predicted bundle strength distributions (several levels i). (d) Asymptotic behaviour in Weibull plots (region from plot (c) highlighted).

Table 1
Nominal model inputs for parametric studies (nominal outputs will be highlighted as ⋄).

Numerical		Mechanical properties					Geometry			Load, k (–)
σ^{max} (GPa)	$\Delta\sigma$ (MPa)	X_m^f (GPa)	CoV_X^f (%)	σ_0^f (GPa)	m (–)	τ_{SL} (MPa)	ϕ^f (μm)	V^f (%)	l_r (mm)	
50	1	4.5	25	4.93	4.54	70	5	60	10	2

Fig. 9 shows that increasing the strength of the matrix/interface strengthens the bundles and reduces strength variability. For very low τ_{SL} values, bundle strength decreases monotonically with bundle level; as the shear-lag strength becomes negligible ($\tau_{SL} \to 0$), the model converges to the WLT (Eq. (2)).

3.4. Asymptotic limits

Varying the stress concentrations factor k (Fig. 10) shows that the model is bounded by the WLT for $k \to \infty$. For $k=1$, a Strongest Link Theory (SLT) applies (a level-$[i+1]$ bundle fails within $l_c^{[i+1]}$ only if no level-$[i]$ bundle survives).

Fig. 11 compares bundle strengths obtained by either (i) running the full model for all bundle levels i or (ii) running the model up to level i^{WLT} followed by the WLT for levels $i > i^{WLT}$ (Eq. (1), with $n = 2^{i-i^{WLT}}$). Although the WLT applied directly to single-fibre ($i^{WLT} = 0$) is extremely inaccurate, both approaches converge if applied from a certain bundle level onwards (in this case, for $i^{WLT} \gtrsim 5$).
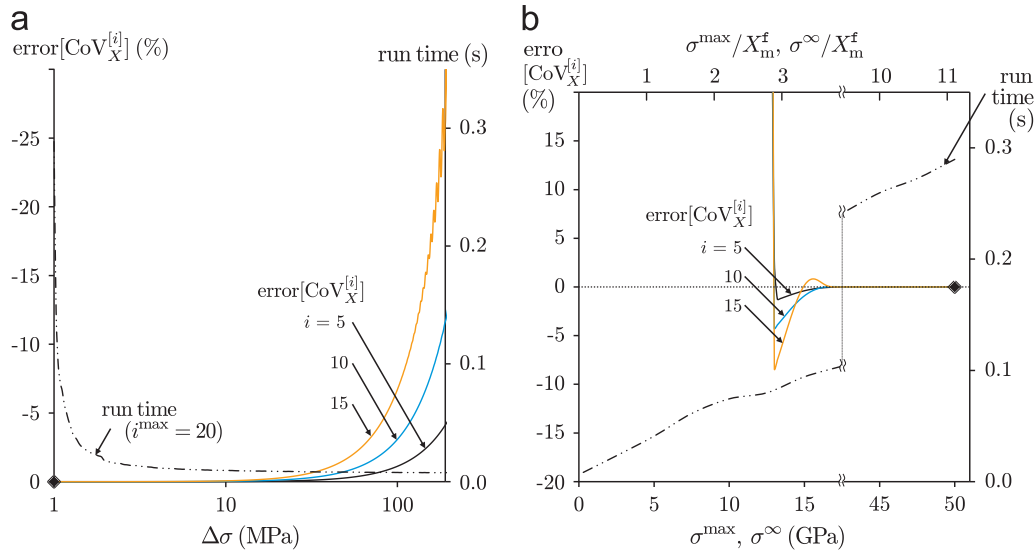
Fig. 6. Numerical convergence of the CoV of strength distributions (for several levels i). Errors are relative to nominal inputs (Table 1), and run times were obtained with an Intel(R) Core(TM)2 Quad CPU at 2.50 GHz, for $i^{max} = 20$ ($n^{[i]} \approx 10^6$). (a) Integration step. (b) Upper integration limit.
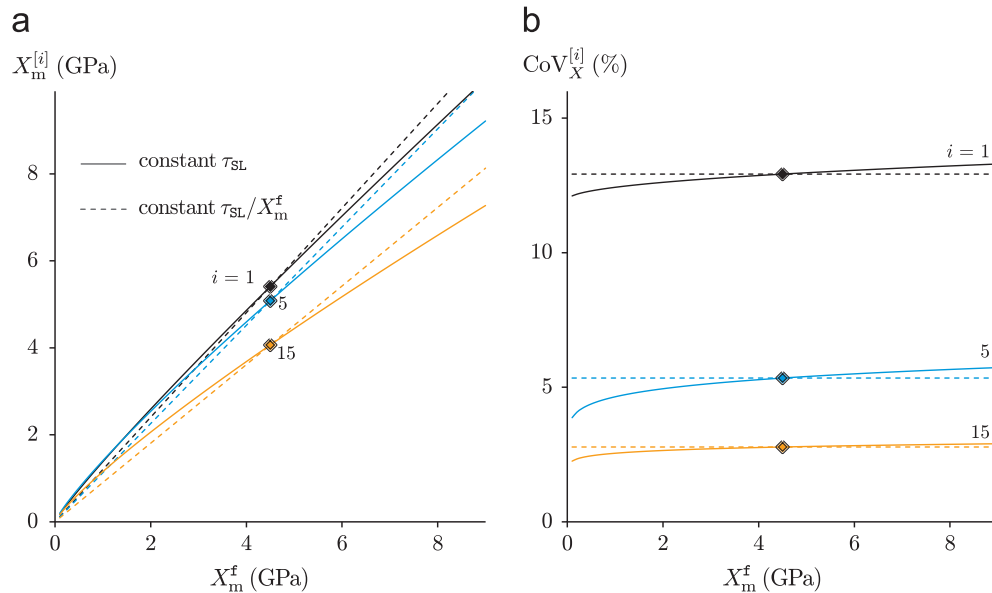

Fig. 7. Effect of mean single-fibre strength on bundle strength statistics (for several levels i). (a) Mean bundle strength. (b) Bundle strength CoV.

3.5. Validation against experimental results

3.5.1. Micro-composites

Fig. 12 validates the model against the experiments from Beyerlein and Phoenix (1996a) and Kazanci (2004) on micro-composites, combining different carbon fibres, epoxy matrices and bundle geometries. Materials and input properties are shown in Tables 2 and 3; single-fibre distributions were fitted as in Fig. 12. Free-edge effects (configuration QB, Appendix A) and a stress concentration factor $k=2$ were considered; strength distributions were obtained directly at $i=2$ for the 4-fibres bundles, and by spline interpolation for the 7-fibres bundles. Each plot presents strength distributions for a fibre type and corresponding bundles (with two different resins); predictions from Newman and Gabrielov's (1991) model are shown for comparison.

3.5.2. Macro-composites

Okabe and Takeda (2002) analysed size effects on the strength of a Toray T800H/3631 (carbon–epoxy) system (Tables 2 and 3) by testing single fibres of several lengths, as well as 10 mm long bundles with $10^4 - 10^6$ fibres. Fig. 13 shows the experimentally measured bundle strengths, together with the strength probability map predicted by the model (the input data used can be found in Tables 2 and 3, and $k=2$); two shear-lag strengths are considered: one at the nominal value
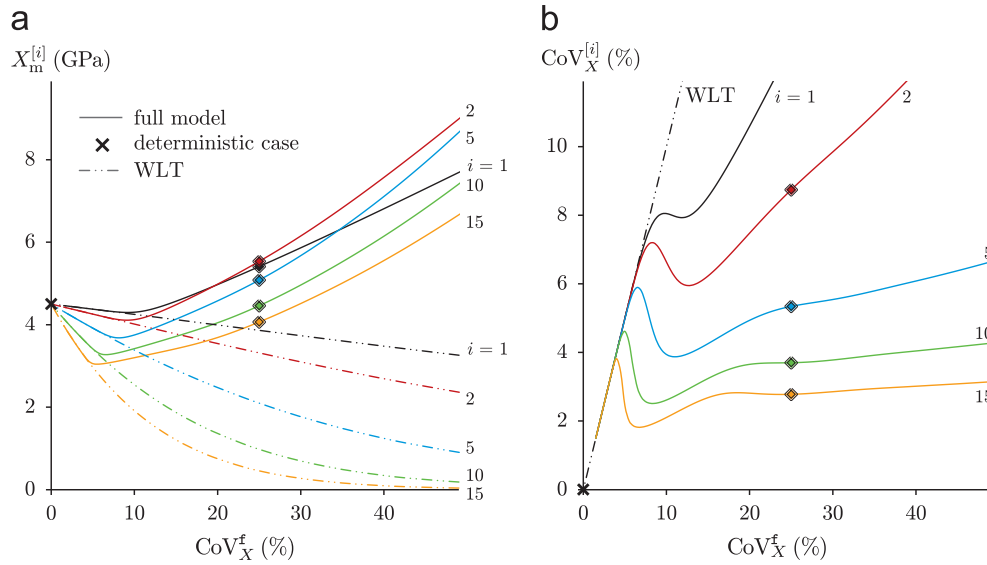
Fig. 8. Effect of the CoV of single-fibre strength on bundle strength statistics (for several levels i). (a) Mean bundle strength. (b) Bundle strength CoV.
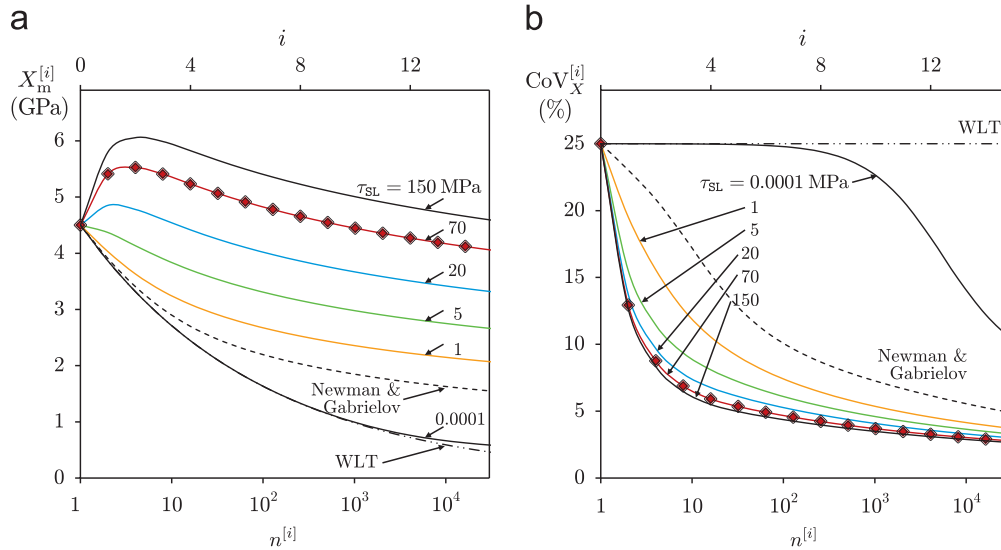

Fig. 9. Bundle strength size effect for several shear-lag strengths (τ_{SL}), and comparison with Newman and Gabrielov's (1991) model and WLT. (a) Mean bundle strength. (b) Bundle strength CoV.

(Fig. 13a) and the other 50% higher (Fig. 13b). Mean bundle strengths predicted by Newman and Gabrielov's (1991) model are shown for comparison.

4. Discussion

4.1. Physically meaningful model features and experimental validation

The model captures many characteristic features of size-effects in the strength of FRPs:

(a) Size effects result from fibre strength variability: Fig. 8 shows no size effect for deterministic fibre strength. The WLT governs damage initiation, but propagation is constrained by the matrix/fibre-matrix interface, which limits stress concentrations and coalescence of fibre breaks.
(b) Both the magnitude of size effects and the variability of tensile strength decrease with increasing specimen size (Wisnom, 1999), as shown by the upwards curvature of $X_m^{[i]}(n^{[i]})$ and $CoV_X^{[i]}(n^{[i]})$ in Fig. 5b (for $i \gtrsim 3$).
(c) The matrix/interface is most important for the micro-scale ($i \lesssim 3$). For most reasonable τ_{SL}, small bundles are stronger than single-fibres (Figs. 9a and 12b). The local geometry influences the strength of small bundles only (Appendix A).
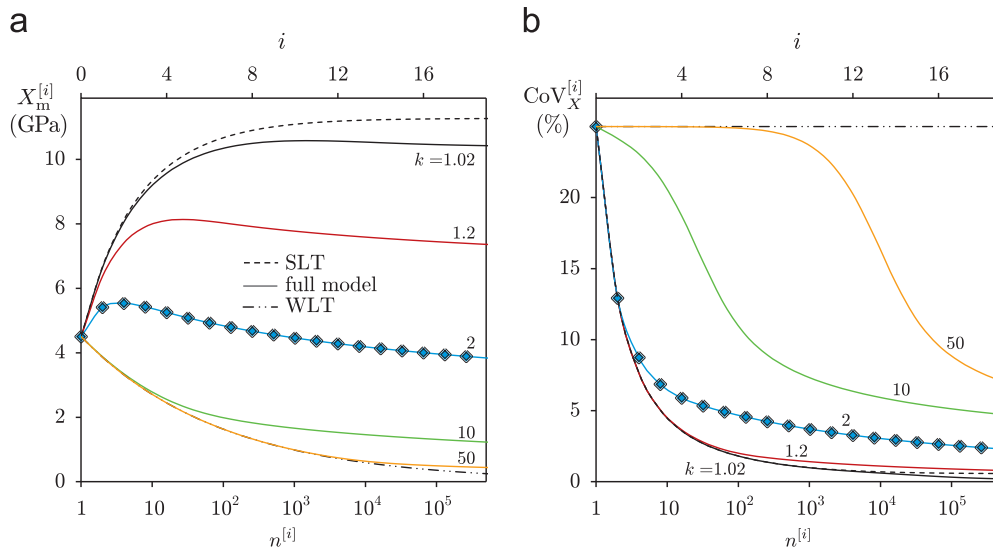
Fig. 10. Bundle strength size effect for different values of the stress concentrations factor k, highlighting the asymptotic limits to the WLT ($k \rightarrow \infty$) and to the SLT ($k=1$). (a) Mean bundle strength. (b) Bundle strength CoV.
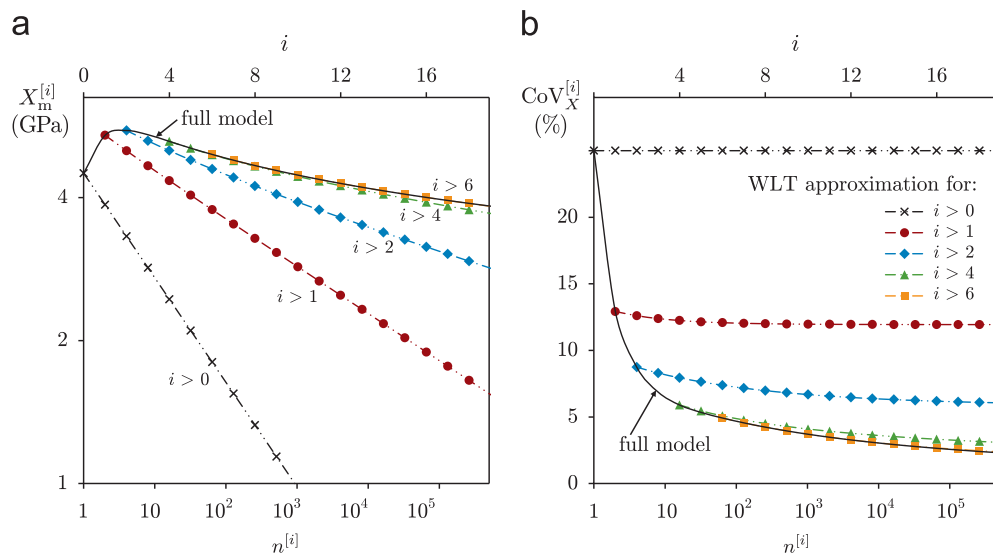

Fig. 11. Bundle strength size effect considering a WLT approximation for large bundles. Note that, for $i^{WLT} > 0$, size effects on the mean strength are not linear in the log–log plot. (a) Mean bundle strength. (b) Bundle strength CoV.

(d) Size effects at the macro-scale ($n^{[i]} \gtrsim 50$) are governed by the WLT (Fig. 11), which is consistent with the quasi-brittle nature of FRPs (Okabe and Takeda, 2002; Scott et al., 2011; Wisnom, 1999). A critical fibre break cluster — after which failure is catastrophic — is defined by the bundle size at which full model and WLT start converging ($n^{[i]} \approx 50$ for the nominal inputs in Table 1).

(e) Within a 0.01–99.99% probability range, predicted large-bundle strength distribution appear quasi-linear in a Weibull plot (Fig. 5c, $i=15$). This agrees with the good fitting usually verified between the Weibull-based WLT and experimental strength distributions and size effects in FRP coupons (Wisnom, 1999).

(f) The model replicates accurately the effect of different fibres and resins on micro-bundle strength distributions (Fig. 12); this offers a strong support to the shear-lag approach used. The model reproduces the concave-down curvature of bundle strength distributions, the different slopes and locations of the four data sets, and the relative orientations within each pair of data for the same fibre type (converging right tails in Fig. 12a, nearly parallel distributions in Fig. 12b).

(g) Fig. 13b evidences a good agreement between predicted and measured strengths in the macro-scale (cross sections up to 30mm², larger than a standard UD FRP tensile-strength specimen, are shown); this implied using a higher shear-lag strength, which is likely to be more representative of the true in situ matrix behaviour (Gulino et al., 1991; Hobbiebrunken et al., 2007).
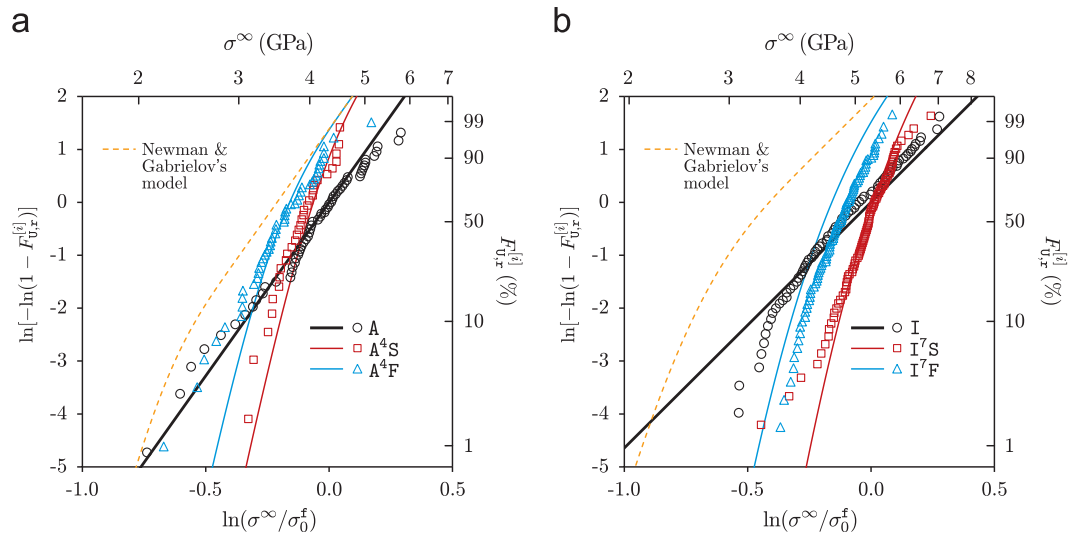
Fig. 12. Micro-composite strength distributions: experimental results (data points from Beyerlein and Phoenix, 1996a; Kazanci, 2004), visually fitted single-fibre distribution for model input (thick lines), present model predictions for both resins types (thin lines), and Newman and Gabrielov's (1991) model prediction (dashed lines). (a) AS4 fibre type ($m=6.6$, $\sigma_0^f = 4.3$ GPa at $l_r = 10$ mm). (b) IM6 fibre type ($m=4.6$, $\sigma_0^f = 5.3$ GPa at $l_r = 10$ mm).

Table 2
Description of composites for model validation.

Ref.	Fibre ref.[a]	$n^{[i]}$	Matrix ref.[b]	τ_{SL} (MPa)	V^f (%)	Reference
A^{4}S	A	4	S	46.6[c]	70	Beyerlein and Phoenix (1996a)
A^{4}F	A	4	F	10.3[c]	70	Beyerlein and Phoenix (1996a)
I^{7}S	I	7	S	46.6[c]	56	Kazanci (2004)
I^{7}F	I	7	F	10.3[c]	56	Kazanci (2004)
T^{n}T	T	10^4–10^6	T	52.4	60	Okabe and Takeda (2002)

[a] See Table 3 for detailed description.
[b] Epoxy resins. Standard (S): DER 331, Dow Plastics; Flexible (F): DER 331 + DER 732 (50:50), Dow Plastics; Toughened (T): 3631, Toray Composites.
[c] Drucker–Prager's criterion, using tensile and compressive strengths (Dow Plastics, 1999).

Table 3
Carbon-fibre data for model validation.

Fibre ref.	Fibre type[a]	ϕ^f (µm)	l_r^f (mm)	$m^{[b]}$	$\sigma_0^{f\,[b]}$ (GPa)	Reference
A	AS4	6.85	10	4.8	4.493	Beyerlein and Phoenix (1996a)
I	IM6	5.63	10	5.4	5.283	Kazanci (2004)
T	T800	5.00	50	3.8	3.570	Okabe and Takeda (2002)

[a] AS4 and IM6 fibres provided by Hercules/Hexcel; T800 fibres provided by Toray.
[b] From the respective Reference, originally calculated through the maximum likelihood method.

4.2. Relation between the present model and others in the literature

4.2.1. Weakest link theory

The present formulation differs from the WLT by considering stable modes of bundle failure (sequences of events E_2 and E_3 in Section 2.3). Consequently, the scaling law (Eq. (11)) degenerates into the WLT (i.e. $S_{U,c}^{[i+1]}(\sigma^\infty) \to S_{U,e}^{[i]}(\sigma^\infty)^4$) whenever these failure modes cannot take place:

(a) Low CoV$_X^f$ (Fig. 8, $\mathcal{C}_K \geq 3$) and/or $k \to \infty$ (Fig. 10). Here, the weakest fibre's neighbour cannot withstand the stress concentrations after first failure.
(b) $\tau_{SL} \to 0$ (Fig. 9). As the scaling law is formulated at the length $l_c^{[i+1]} \propto 1/\tau_{SL}$, this case degenerates into a dry (loose) bundle with infinite length under local load sharing, governed by the WLT.
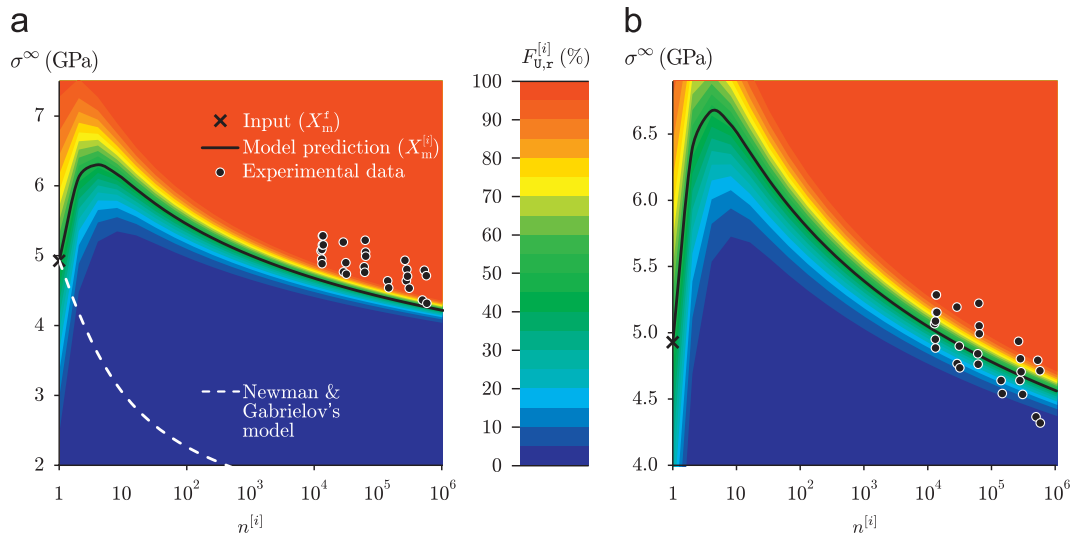
Fig. 13. Macro-bundle strengths for model validation: experimental bundle strengths (data points from Okabe and Takeda, 2002), present model's probability map (with mean strength highlighted), and Newman and Gabrielov's (1991) mean strength prediction (dashed line in (a)). (a) $\tau_{SL} = 52.4$ MPa (nominal). (b) $\tau_{SL} = 79.6$ MPa (50% stronger).

(c) Large i or $n^{[i]}$ (Fig. 11). As strength variability decreases with increasing bundle size (Fig. 5b), failure of a sufficiently large sub-bundle immediately triggers failure of its neighbour.

4.2.2. Newmanand and Gabrielov's (1991) model

The present model shows key differences to the one originally developed by Newman and Gabrielov (1991, Eq. (3)):

(a) This model considers a shear-lag boundary; this confines stress concentrations around fibre breaks, and defines a characteristic length ($l_c^{[i]}$, generally shorter than the original bundle length). Consequently, the present model predicts higher mean bundle strength and lower variability (Fig. 5b).
(b) As the characteristic length is fundamental for size effects in quasi-brittle materials (Bažant, 1999), the present work shows a much better correlation with experiments in FRPs (Figs. 12 and 13) than the original model from Newman and Gabrielov, which was developed for dry fibre bundles.
(c) Such characteristic length makes this model consistent with the WLT for length scaling. On the contrary, applying Newman and Gabrielov's (1991) model to bundles of different lengths yields strength distributions which cannot be related to the WLT.
(d) For extremely weak matrices, the present model converges not to Newman and Gabrielov's model directly, but to its asymptotic limit for large bundles — the WLT (Fig. 9). This is again due to using $l_c^{[i+1]} \propto 1/\tau_{SL}$ as characteristic length.
(e) Newman and Gabrielov reduced the order of their scaling law by re-organising the computations. Instead, this was addressed in the present model by using an asymptotic result (Eq. (18)), which would be applicable to the former model as well.

4.2.3. Fibre-bundle models

The central aspects relating the present model and other fibre-bundle models in the literature are discussed below:

(a) Analytical fibre-bundle models with local load sharing become prohibitively complex for bundles with more than 10 fibres (Harlow and Phoenix, 1978a); this has been overcome in the literature through asymptotic simplifications (Curtin, 1993, Phoenix et al. 1997, 1988, Phoenix and Smith, 1983) and Monte-Carlo simulations (Landis et al., 2000; Mahesh et al., 2002; Okabe and Takeda, 2001; Wada and Fukuda, 1999). The present model is made suitable to a complete range of scales (Fig. 5) by the use of hierarchies and an efficient implementation scheme; still, the typical features of fibre bundle models are captured—namely size effects and the existence of a critical cluster of fibre breaks (Fig. 11).
(b) Several authors (Behzadi et al., 2009; Landis et al., 2000; Mahesh et al., 2002; Phoenix et al., 1988) recognised that, although their models used a fixed characteristic length, this is not realistic nor accurate; Wisnom and Green (1995) considered the characteristic length to be additive regarding the number of broken fibres, but included no stress concentrations in their calculations. The present model uses a variable control length $l_c^{[i+1]}$ (Eq. (12)) that depends on the level of the broken cluster; this is in agreement with experimental observations of self-similar fracture surfaces in FRPs (Laffan et al., 2010; Pimenta et al., 2010).

(c) This model uses simple definitions of load transfer and characteristic length (Eq. (12)), as well as a constant stress concentration factor ($k=2$ from equilibrium of forces). Other definitions can be explored, namely on the matrix response (Nairn, 1997; Okabe and Takeda, 2001), the size of l_c (Phoenix et al., 1997), and magnitude of stress concentrations (Beyerlein and Phoenix, 1996b; Hedgepeth, 1961; Nedele and Wisnom, 1994). However, these are still unresolved topics in the literature, hence justifying the use of simplified approaches.

5. Conclusions

An analytical model for size effects on the longitudinal tensile strength of FRP bundles was developed, implemented and validated. The model is based on the stochastic analysis of the failure process in hierarchical fibre bundles, considering Weibull fibre-strength distributions. Matrix effects are represented through a simplified shear-lag model, so that the *control length* (in which fibre breaks interact) scales hierarchically as well.

The model predicts full strength distributions and statistics for bundles of any size. The matrix (or fibre–matrix interface) was shown to have a significant strengthening effect, which supports the present model over others not including this feature (e.g. WLT and Newman and Gabrielov, 1991). An efficient numerical scheme was proposed, leading to full-model running times below one second.

The model was validated both at the micro- and macro-scales, showing a remarkable agreement with experimentally measured bundle strengths in a large range of sizes. The quasi-brittle nature of composites is reproduced; the model also illustrates many experimentally observed trends, such as the tensile strength of FRPs appearing to follow a Weibull distribution, and large-scale size effects consistent with the WLT.

Predictive models for size effects in composite materials are paramount for scaling small-coupon experimental results to the design of large structures. In addition to such quantitative predictions, the present work provides insight on the longitudinal tensile failure process. The model's ability to compute strength distributions for small bundles (rather than only for asymptotically large ones) makes it particularly suitable for state-of-the-art multiscale discontinuous-fibre composites. This model has also been applied to predict the fracture toughness of FRPs under longitudinal tensile failure (Pimenta and Pinho, submitted for publication).

Acknowledgments

Appendix A. Effect of bundle and shear-lag boundary geometry on strength

Table A1 defines alternative geometries for the shear-lag boundary, taking into account different fibre arrangements, failure paths and free-edge effects.

Matching the perimeter of these different geometries with the corresponding mean bundle strength (Fig. A1) reveals that the largest shear-lag boundary at low-level bundles (QM geometry) yields the strongest bundles throughout the whole hierarchy. On the contrary, a large boundary at high-level bundles (HI geometry) yields no strengthening effect. Free-boundary effects (QB vs. QI geometries) affect small bundles only.

All these observations support that (i) the shear-lag boundary plays a critical role for the strength of small-scale bundles, while (ii) the weakest link theory dominates size effects for large-scale bundles (see Section 4.1 for further discussion).

Appendix B. Generalisation of the weakest link theory to non-uniform stress fields

The weakest link theory (Eq. (1)) can be generalised to non-uniform stress fields. Consider a chain composed by n elements, each of length l_r and under a uniform tensile stress σ_j, $j = \{1 \ldots n\}$. The chain (of length $l_n = n \cdot l_r$) is subjected to a piecewise constant but otherwise generic stress field Φ, with survival probability $S_{\Phi,n}$ related to those of the uniformly loaded element ($S_{U,r}$) and the chain with same length ($S_{U,n}$):

$$S_{\Phi,n} = \prod_{j=1}^{n} S_{U,r}(\sigma_j) \quad \overset{\text{Eq. (1)}}{\Rightarrow} \quad \ln[S_{\Phi,n}] = \sum_{j=1}^{n} \frac{l_r}{l_n} \cdot \ln[S_{U,n}(\sigma_j)] \tag{B.1}$$

This relation can be applied to a fibre or bundle of length l under a linear stress field (defined by the variable remote stress σ^∞ and fixed stress concentration factor k, e.g. segment $\mathcal{B}_1$ in Fig. 3a):

$$\sigma_K(x) = \sigma^\infty + \frac{\sigma^\infty \cdot (k-1)}{l} \cdot x, \quad x \in [0,l] \tag{B.2}$$

Dividing the chain into $n \to \infty$ links of length $\Delta x = l/n$, the survival probability S_{K} of the chain under $\sigma_{\mathrm{K}}(x)$ relates to that of a uniformly loaded chain (S_{U}) by:

$$\ln[S_{\mathrm{K}}] = \lim_{n \to \infty} \sum_{j=1}^{n} \frac{\Delta x}{l} \cdot \ln[S_{\mathrm{U}}(\sigma_{\mathrm{K}}(x_j))] = \frac{1}{l} \int_{x=0}^{l} \ln[S_{\mathrm{U}}(\sigma_{\mathrm{K}}(x))] \, \mathrm{d}x \tag{B.3}$$

Table A1
Alternative definitions of the shear-lag boundary.

Perimeters in square arrangement were derived for even values of i (with $n^{[i]} = 2^i$); perimeters in hexagonal arrangement were derived for integer values of the hexagonal level i_{H} (with $n^{[i]} = 7^{i_{\mathrm{H}}} = 2^i$).

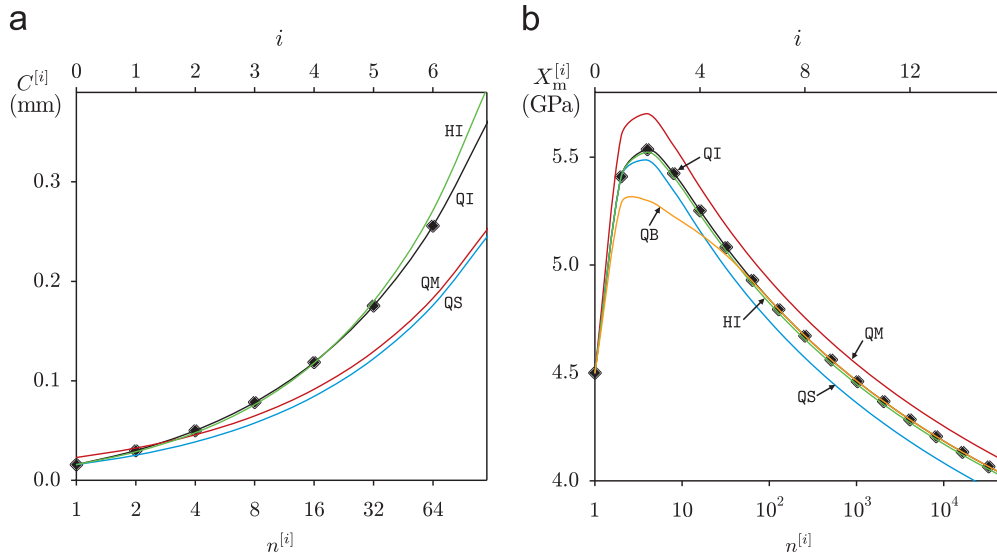| Ref.	Description and perimeter $C^{[i]}$	Diagram
QM	Square fibre arrangement, preferential matrix failure: $$C_{\mathrm{QM}}^{[i]} = 4 \cdot \sqrt{n^{[i]}} \cdot l_{\mathrm{Q}} \quad \text{with } l_{\mathrm{Q}} = \frac{\sqrt{\pi} \cdot \phi^{\mathrm{f}}}{2 \cdot \sqrt{V^{\mathrm{f}}}} \tag{A.1}$$	
QI	Square fibre arrangement, preferential interfacial failure (default configuration, Eq. (5) in Section 2.1): $$C_{\mathrm{QI}}^{[i]} = 3 \cdot C^{\mathrm{f}} + 4 \cdot \left[(\sqrt{n^{[i]}} - 1) \cdot s_{\mathrm{Q}} + (\sqrt{n^{[i]}} - 2) \cdot \frac{C^{\mathrm{f}}}{2} \right] \tag{A.2}$$	
QS	Square fibre arrangement, shortest failure path: $$C_{\mathrm{QS}}^{[i]} = C^{\mathrm{f}} + 4 \cdot (\sqrt{n^{[i]}} - 1) \cdot l_{\mathrm{Q}} \tag{A.3}$$	
HI	Hexagonal fibre arrangement, preferential interfacial failure (fractal boundary, hence initial recursive relation): $$C_{\mathrm{HI}}^{[i_{\mathrm{H}}]} = 6 \cdot \left(\frac{C_{\mathrm{HI}}^{[i_{\mathrm{H}}-1]}}{2} + \frac{C^{\mathrm{f}}}{6} + s_{\mathrm{H}} \right) \quad \text{with } s_{\mathrm{H}} = \left(\sqrt{\frac{\pi}{2\sqrt{3}V^{\mathrm{f}}}} - 1 \right) \cdot \phi^{\mathrm{f}}$$ $$C_{\mathrm{HI}}^{[i_{\mathrm{H}}]} = 3^{i_{\mathrm{H}}} \cdot C^{\mathrm{f}} + \frac{3^{i_{\mathrm{H}}} - 1}{2} \cdot (C^{\mathrm{f}} + 6 \cdot s_{\mathrm{H}})$$ $$C_{\mathrm{HI}}^{[i_{\mathrm{H}}]} \equiv C_{\mathrm{HI}}^{[i]} = 3 \cdot (\sqrt[\log 3]{7} n^{[i]} - 1) \cdot s_{\mathrm{H}} + (3 \cdot \sqrt[\log 3]{7} n^{[i]} - 1) \cdot \frac{C^{\mathrm{f}}}{2} \tag{A.4}$$	hexagonal level $i_{\mathrm{H}} = 1$ $i_{\mathrm{H}} = 2$
QB	Square fibre arrangement, preferential interfacial failure, considering free-edge effects in levels $i^{\max}-2$ and $i^{\max}-1$ (configuration QI should be used up to level $i^{\max}-3$): $$C_{\mathrm{QB,edge}}^{[i^{\max}-1]} = \sqrt{2 \cdot n^{[i]}} \cdot \left(s_{\mathrm{Q}} + \frac{C^{\mathrm{f}}}{2} \right) \quad \text{with } s_{\mathrm{Q}} = \left(\frac{\sqrt{\pi}}{2\sqrt{V^{\mathrm{f}}}} - 1 \right) \cdot \phi^{\mathrm{f}} \tag{A.5}$$ $$C_{\mathrm{QB,corner}}^{[i^{\max}-2]} = \frac{C^{\mathrm{f}}}{4} + 2 \cdot \left(\sqrt{n^{[i]}} - \frac{1}{2} \right) \cdot \left(s_{\mathrm{Q}} + \frac{C^{\mathrm{f}}}{2} \right) \tag{A.6}$$	free boundary $i = i^{\max}$ edge boundary $i = i^{\max} - 1$ corner boundary $i = i^{\max} - 2$

a

b

Fig. A1. Bundle strength size effect for several shear-lag geometries. (a) Shear-lag boundary perimeter. (b) Mean bundle strength.

Changing the integration variable from x to σ_{K} (using the field in Eq. (B.2)),

$$\ln\left[S_{\mathrm{K}}(\sigma^{\infty})\right] = \begin{cases} \dfrac{1}{\sigma^{\infty} \cdot (k-1)} \displaystyle\int_{\sigma_{\mathrm{K}}=\sigma^{\infty}}^{k \cdot \sigma^{\infty}} \ln\left[S_{\mathrm{U}}(\sigma_{\mathrm{K}})\right] \mathrm{d}\sigma_{\mathrm{K}} & \text{if } k > 1 \\ \ln\left[S_{\mathrm{U}}(\sigma^{\infty})\right] & \text{if } k = 1 \end{cases} \tag{B.4}$$

A similar procedure can be applied to a pure linear stress field $\sigma_{\mathrm{L}}(x)$, under which the chain survival probability is then S_{L}

$$\sigma_{\mathrm{L}}(x) = \frac{\sigma^{\infty}}{l} \cdot x, \quad x \in [0,l] \Rightarrow \ln\left[S_{\mathrm{L}}(\sigma^{\infty})\right] = \frac{1}{\sigma^{\infty}} \int_{\sigma_{\mathrm{L}}=0}^{\sigma^{\infty}} \ln\left[S_{\mathrm{U}}(\sigma_{\mathrm{L}})\right] \mathrm{d}\sigma_{\mathrm{L}} \tag{B.5}$$

Combining both previous equations, $S_{\mathrm{K}}(\sigma^{\infty})$ can also be defined by:

$$\ln\left[S_{\mathrm{K}}(\sigma^{\infty})\right] = \begin{cases} \dfrac{k \cdot \ln\left[S_{\mathrm{L}}(k \cdot \sigma^{\infty})\right] - \ln\left[S_{\mathrm{L}}(\sigma^{\infty})\right]}{k-1} & \text{if } k > 1 \\ \ln\left[S_{\mathrm{U}}(\sigma^{\infty})\right] & \text{if } k = 1 \end{cases} \tag{B.6}$$

Eqs. (B.4)–(B.6) are valid regardless of the shape of the strength distribution $S_{\mathrm{U}}(\sigma^{\infty})$. For the particular case of a Weibull distribution with parameters m and σ_0,

$$\ln\left[S_{\mathrm{K}}(\sigma^{\infty})\right] = \mathcal{C}_{\mathrm{K}} \cdot \ln\left[S_{\mathrm{U}}(\sigma^{\infty})\right] \Rightarrow S_{\mathrm{K}}(\sigma^{\infty}) = \exp\left[-\mathcal{C}_{\mathrm{K}} \cdot \left(\frac{\sigma^{\infty}}{\sigma_0}\right)^m\right] \quad \text{where } \mathcal{C}_{\mathrm{K}} = \frac{k^{m+1}-1}{(m+1)(k-1)} \tag{B.7}$$

Appendix C. Physically – based derivation of the hierarchical scaling law

The scaling law in Eq. (8) can be derived from the physically reasonable sequences of events E_1, E_2 and E_3 defined in Section 2.3. This requires extending the concept of stochastic strength of a fibre segment to the linear stress concentrations field that occurs near a fibre break (Fig. 3).

Consider the stress field after failure of segment $\mathcal{A}_1$ in a level-[1] bundle (Fig. 3a). Let $X_{\mathrm{U,e}}^{\mathcal{B}_2}$ be the stochastic strength of the fibre segment $\mathcal{B}_2$ under uniform stresses (indicated by the subscript U); $\mathcal{B}_2$ fails if $X_{\mathrm{U,e}}^{\mathcal{B}_2} \leq \sigma^{\infty}$. Similarly, $X_{\mathrm{K,e}}^{\mathcal{B}_1}$ is the stochastic strength of the segment $\mathcal{B}_1$ under linear stress concentrations, characterised by a variable remote stress σ^{∞} and constant factor k; $\mathcal{B}_1$ fails if $X_{\mathrm{K,e}}^{\mathcal{B}_1} \leq \sigma^{\infty}$.

The sequences of events leading to bundle failure (E_1, E_2 and E_3) can now be formally defined as:

E_1: *Unstable bundle failure* at $\sigma^{\infty} = X_{\mathrm{U,c}}^{[1]}$. All 4 segments survive the uniform stress field for $\sigma^{\infty} < X_{\mathrm{U,c}}^{[1]}$; $\mathcal{A}_1$ fails when $\sigma^{\infty} = X_{\mathrm{U,c}}^{[1]}$, triggering failure of $\mathcal{B}_1$ due to stress concentrations. Formally,

$$E_1 = \{\sigma^{\infty} : [X_{\mathrm{U,e}}^{\mathcal{A}_1} = \sigma^{\infty}] \wedge [X_{\mathrm{U,e}}^{\mathcal{A}_2} > \sigma^{\infty}] \wedge [X_{\mathrm{U,e}}^{\mathcal{B}_1} > \sigma^{\infty} \wedge X_{\mathrm{K,e}}^{\mathcal{B}_1} \leq \sigma^{\infty}] \wedge [X_{\mathrm{U,e}}^{\mathcal{B}_2} > \sigma^{\infty}]\} \tag{C.1}$$

E_2: *Stable bundle failure due to stress concentrations* at $\sigma^\infty = X_{U,c}^{[1]}$. $\mathcal{A}_1$ fails when $\sigma^\infty = X_{U,e}^{\mathcal{A}} < X_{U,c}^{[1]}$, and (from the assumption A(ii)) $\mathcal{A}_2$ survives $\sigma^\infty \leq X_{U,e}^{\mathcal{A}}$. $\mathcal{B}_2$ withstands the stress field for $\sigma^\infty \leq X_{U,c}^{[1]}$, but $\mathcal{B}_1$ fails under stress concentrations at $\sigma^\infty = X_{U,c}^{[1]}$. Formally,

$$E_2 = \{\sigma^\infty : [X_{U,e}^{\mathcal{A}_1} < \sigma^\infty] \wedge [X_{U,e}^{\mathcal{A}_2} > X_{U,e}^{\mathcal{A}_1}] \wedge [X_{K,e}^{\mathcal{B}_1} = \sigma^\infty] \wedge [X_{U,e}^{\mathcal{B}_2} > \sigma^\infty]\} \tag{C.2}$$

E_3: *Stable bundle failure due to independent fibre flaws* at $\sigma^\infty = X_{U,c}^{[1]}$. $\mathcal{A}_1$ fails when $\sigma^\infty = X_{U,e}^{\mathcal{A}} < X_{U,c}^{[1]}$, and $\mathcal{A}_2$ survives $\sigma^\infty \leq X_{U,e}^{\mathcal{A}}$. $\mathcal{B}_1$ withstands the stress concentrations field for $\sigma^\infty \leq X_{U,c}^{[1]}$, but $\mathcal{B}_2$ fails under uniform stresses at $\sigma^\infty = X_{U,c}^{[1]}$, either due to a stress increment $d\sigma^\infty$ or domain extension $dl_e(\sigma^\infty)$ (from Eq. (6)):

$$E_3 = \{\sigma^\infty : [X_{U,e}^{\mathcal{A}_1} < \sigma^\infty] \wedge [X_{U,e}^{\mathcal{A}_2} > X_{U,e}^{\mathcal{A}_1}] \wedge [X_{K,e}^{\mathcal{B}_1} > \sigma^\infty] \wedge [X_{U,e}^{\mathcal{B}_2} = \sigma^\infty]\} \tag{C.3}$$

The events above assume the weakest segment in the control length is $\mathcal{A}_1$ which (without loss of generality) represents 1/4 of the cases. Therefore, the level-[1] bundle strength distribution within the control length is

$$\Pr(X_{U,c}^{[1]} = \sigma^\infty) = 4 \cdot [\Pr(E_1) + \Pr(E_2) + \Pr(E_3)] \tag{C.4}$$

The probability for each sequence of events E_1, E_2 and E_3 is defined from the single-fibre strength distributions. All fibre segments have independent and identically distributed strengths; therefore, failure probabilities (cumulative distribution functions) under uniform stresses and under linear stress concentrations are represented respectively as $F_{U,e}^{[0]}(\sigma^\infty) = \Pr(X_{U,e}^{\mathcal{B}_2} \leq \sigma^\infty)$ and $F_{K,e}^{[0]}(\sigma^\infty) = \Pr(X_{K,e}^{\mathcal{B}_1} \leq \sigma^\infty)$. Consequently:

$$\Pr(E_1) \overset{\text{Eq. (C.1)}}{=} [dF_{U,e}^{[0]}(\sigma^\infty)] \cdot [1 - F_{U,e}^{[0]}(\sigma^\infty)] \cdot [F_{K,e}^{[0]}(\sigma^\infty) - F_{U,e}^{[0]}(\sigma^\infty)] \cdot [1 - F_{U,e}^{[0]}(\sigma^\infty)]$$

$$\Pr(E_2) \overset{\text{Eq. (C.2)}}{=} \int_{\sigma = 0}^{\sigma^\infty} ([dF_{U,e}^{[0]}(\sigma)] \cdot [1 - F_{U,e}^{[0]}(\sigma)]) \cdot [dF_{K,e}^{[0]}(\sigma^\infty)] \cdot [1 - F_{U,e}^{[0]}(\sigma^\infty)]$$
$$= [F_{U,e}^{[0]}(\sigma^\infty)] \cdot [1 - F_{U,e}^{[0]}(\sigma^\infty)/2] \cdot [dF_{K,e}^{[0]}(\sigma^\infty)] \cdot [1 - F_{U,e}^{[0]}(\sigma^\infty)]$$

$$\Pr(E_3) \overset{\text{Eq. (C.3)}}{=} [F_{U,e}^{[0]}(\sigma^\infty)] \cdot [1 - F_{U,e}^{[0]}(\sigma^\infty)/2] \cdot [1 - F_{K,e}^{[0]}(\sigma^\infty)] \cdot [dF_{U,e}^{[0]}(\sigma^\infty)] \tag{C.5}$$

The level-[1] bundle strength distribution $F_{U,c}^{[1]}(\sigma^\infty)$ is calculated by replacing the probabilities above in Eq. (C.4), and integrating $\Pr(X_{U,c}^{[1]} = \sigma)$ for all $\sigma \leq \sigma^\infty$:

$$F_{U,c}^{[1]}(\sigma^\infty) = 4 \cdot \int_{\sigma = 0}^{\sigma^\infty} [dF_{U,e}^{[0]}(\sigma) \cdot [1 - F_{U,e}^{[0]}(\sigma)] \cdot [F_{K,e}^{[0]}(\sigma) - F_{U,e}^{[0]}(\sigma)] \cdot [1 - F_{U,e}^{[0]}(\sigma)]$$
$$+ F_{U,e}^{[0]}(\sigma) \cdot [1 - F_{U,e}^{[0]}(\sigma)/2] \cdot dF_{K,e}^{[0]}(\sigma) \cdot [1 - F_{U,e}^{[0]}(\sigma)] + F_{U,e}^{[0]}(\sigma) \cdot [1 - F_{U,e}^{[0]}(\sigma)/2] \cdot [1 - F_{K,e}^{[0]}(\sigma)] \cdot dF_{U,e}^{[0]}(\sigma)] \tag{C.6}$$

Recalling that $F^N dF = d(F^{N+1})/(N+1)$ and re-arranging the equation (omitting the integration variable σ and the single-fibre superscript [0] for readability) yields

$$F_{U,c}^{[1]}(\sigma^\infty) = -F_{U,e}(\sigma^\infty)^4 + 2 \cdot F_{U,e}(\sigma^\infty)^3 + 2 \cdot \left[\int F_{K,e} \, d(F_{U,e}^3) + \int F_{U,e}^3 \, dF_{K,e} \right]_{\sigma = 0}^{\sigma^\infty}$$
$$- 6 \cdot \left[\int F_{K,e} \cdot (F_{U,e}^2) + \int F_{U,e}^2 \, dF_{K,e} \right]_{\sigma = 0}^{\sigma^\infty} + 4 \cdot \left[\int F_{K,e} \, dF_{U,e} + \int F_{U,e} \, dF_{K,e} \right]_{\sigma = 0}^{\sigma^\infty} \tag{C.7}$$

Integrating by parts each pair of integrals results into

$$F_{U,c}^{[1]}(\sigma^\infty) = -F_{U,e}^{[0]}(\sigma^\infty)^4 + 2 \cdot F_{U,e}^{[0]}(\sigma^\infty)^3 + 2 \cdot F_{U,e}^{[0]}(\sigma^\infty)^3 \cdot F_{K,e}^{[0]}(\sigma^\infty)$$
$$- 6 \cdot F_{U,e}^{[0]}(\sigma^\infty)^2 \cdot F_{K,e}^{[0]}(\sigma^\infty) + 4 \cdot F_{U,e}^{[0]}(\sigma^\infty) \cdot F_{K,e}^{[0]}(\sigma^\infty) \tag{C.8}$$

Converting all distributions to survival probabilities, $S(\sigma^\infty) = 1 - F(\sigma^\infty)$, this corresponds to the scaling law proposed in Eq. (8) of Section 2.3.

Appendix D. Proof of asymptotic behaviour for strength distributions

D.1. Right tail asymptote

Assuming single-fibre strength follows a Weibull distribution (thus $\ln[S_{K,r}^{[0]}] = \mathcal{C}_K \cdot \ln[S_{U,r}^{[0]}]$ from Eq. (B.7)), applying the scaling law (Eq. (14)) to $i=0$ yields

$$\ln(S_{U,r}^{[1]}) = 2 \cdot \ln(S_{U,r}^{[0]}) + \frac{l_r}{2 \cdot l_e^{[0]}} \cdot \ln(1 + 2 \cdot [S_{U,r}^{[0]}]^{(\mathcal{C}_K - 3) \cdot l_e^{[0]}/l_r} - 2 \cdot [S_{U,r}^{[0]}]^{(\mathcal{C}_K - 1) \cdot l_e^{[0]}/l_r})$$
$$= \frac{(1 + \mathcal{C}_K) \cdot \ln(S_{U,r}^{[0]})}{2} + \frac{l_r}{2 \cdot l_e^{[0]}} \cdot \ln(2 + [S_{U,r}^{[0]}]^{(3 - \mathcal{C}_K) \cdot l_e^{[0]}/l_r} - 2 \cdot [S_{U,r}^{[0]}]^{2 \cdot l_e^{[0]}/l_r}) \tag{D.1}$$

For large stresses, $S_{U,r}^{[0]}(\sigma^\infty) \to 0$ and $l_e^{[0]} \to \infty$ (Eqs. (6) and (9)), so the contribution of the terms highlighted above vanishes (as long as exponents are positive). Therefore,

$$\lim_{\sigma^\infty \to \infty} \ln[S_{U,r}^{[1]}(\sigma^\infty)] = \psi \cdot \ln[S_{U,r}^{[0]}(\sigma^\infty)] \Rightarrow \lim_{\sigma^\infty \to \infty} S_{U,r}^{[1]}(\sigma^\infty) = \exp\left[-\psi \cdot \left(\frac{\sigma^\infty}{\sigma_0^f}\right)^m\right] \quad \text{with } \psi = \begin{cases} 2, & \mathcal{C}_K \geq 3 \\ \dfrac{1+\mathcal{C}_K}{2}, & \mathcal{C}_K < 3 \end{cases} \tag{D.2}$$

The right tail asymptote of $S_{U,r}^{[1]}$ is recognisably a Weibull distribution. Consequently, the same argument can be applied recursively up to any level-[i] bundle, whose right tail will then tend asymptotically to a Weibull distribution as well (ψ as defined above):

$$\lim_{\sigma^\infty \to \infty} \ln[S_{U,r}^{[i]}(\sigma^\infty)] = \psi \cdot \ln[S_{U,r}^{[i-1]}(\sigma^\infty)] \Rightarrow \lim_{\sigma^\infty \to \infty} S_{U,r}^{[i]}(\sigma^\infty) = \exp\left[-\psi^i \cdot \left(\frac{\sigma^\infty}{\sigma_0^f}\right)^m\right] \tag{D.3}$$

D.2. Left tail asymptote

The single-fibre survival probabilities at the effective recovery length can be expressed as (Eqs. (6), (9) and (10))

$$S_{U,e}^{[0]}(\sigma^\infty) = \exp(-u^{[0]}) \quad \text{and} \quad S_{K,e}^{[0]}(\sigma^\infty) = \exp(-\mathcal{C}_K \cdot u^{[0]}) \quad \text{with } u^{[0]} = \frac{l_e^{[0]}}{l_r} \cdot \left(\frac{\sigma^\infty}{\sigma_0^f}\right)^m \tag{D.4}$$

According to the scaling law in Eq. (8), the level-[1] survival probability in the control length becomes

$$S_{U,c}^{[1]}(\sigma^\infty) = \exp[-4 \cdot u^{[0]}] + 2 \cdot \exp[-(1+\mathcal{C}_K) \cdot u^{[0]}] - 2 \cdot \exp[-(3+\mathcal{C}_K) \cdot u^{[0]}] \tag{D.5}$$

Taking the limit for low stresses, and using the 2nd order Taylor expansion of the exponential function — $\lim_{\psi \to 0} \exp(\psi) = 1 + \psi + \psi^2/2$ — then

$$\lim_{\sigma^\infty \to 0} S_{U,c}^{[1]}(\sigma^\infty) = (1 - 4 \cdot u^{[0]} + [4 \cdot u^{[0]}]^2/2) + 2 \cdot (1 - (1+\mathcal{C}_K) \cdot u^{[0]} + [(1+\mathcal{C}_K) \cdot u^{[0]}]^2/2)$$

$$-2 \cdot (1 - (3+\mathcal{C}_K) \cdot u^{[0]} + [(3+\mathcal{C}_K) \cdot u^{[0]}]^2/2) = 1 - 4 \cdot \mathcal{C}_K \cdot (u^{[0]})^2$$

$$= \lim_{\sigma^\infty \to 0} \exp[-4 \cdot \mathcal{C}_K \cdot (u^{[0]})^2] = \lim_{\sigma^\infty \to 0} \exp\left[-4 \cdot \mathcal{C}_K \cdot \left(\frac{l_e^{[0]}}{l_r}\right)^2 \cdot \left(\frac{\sigma^\infty}{\sigma_0^f}\right)^{2 \cdot m}\right] \tag{D.6}$$

Scaling from $l_c^{[1]}$ (Eq. (7)) to the reference length (WLT as in Eq. (1)),

$$\lim_{\sigma^\infty \to 0} S_{U,r}^{[1]}(\sigma^\infty) = \exp\left[-2 \cdot \mathcal{C}_K \cdot \frac{l_e^{[0]}}{l_r} \cdot \left(\frac{\sigma^\infty}{\sigma_0^f}\right)^{2 \cdot m}\right] = \exp\left[-4 \cdot \mathcal{C}_K \cdot \frac{A^f \cdot \sigma_0^f}{C^{[0]} \cdot \tau_{SL}} \cdot \left(\frac{\sigma^\infty}{\sigma_0^f}\right)^{2 \cdot m+1}\right] \tag{D.7}$$

This shows that the left tail asymptote of a level-[1] strength distribution preserves the Weibull nature of the single-fibre distribution (although with different parameters). Consequently, the same argument can be applied recursively up to any level-[i] bundle, hence its left tail Weibull parameters ($m_{LTA}^{[i]}$ and $\sigma_{0,LTA}^{[i]}$) are related to those of a level-[i−1] bundle by

$$m_{LTA}^{[i]} = 2 \cdot m_{LTA}^{[i-1]} + 1 \quad \text{and} \quad \sigma_{0,LTA}^{[i]} = \sigma_{0,LTA}^{[i-1]} \cdot \left(4 \cdot \mathcal{C}_{K,LTA}^{[i-1]} \cdot \frac{n^{[i-1]} \cdot A^f \cdot \sigma_{0,LTA}^{[i-1]}}{C^{[i-1]} \cdot \tau_{SL} \cdot l_r}\right)^{-1/m_{LTA}^{[i]}}$$

$$\text{with } \mathcal{C}_{K,LTA}^{[i]} = \frac{k^{m_{LTA}^{[i]}+1} - 1}{(m_{LTA}^{[i]}+1) \cdot (k-1)} \text{ and } m_{LTA}^{[0]} = m, \quad \sigma_{0,LTA}^{[0]} = \sigma_0^f \tag{D.8}$$

References

Accorsi, M.L., Pegoretti, A., Dibenedetto, A.T., 1996. Dynamic analysis of fibre breakage in single- and multiple-fibre composites. J. Mater. Sci. 31, 4181–4187.

Bažant, Z.P., 1999. Size effect on structural strength: a review. Arch. Appl. Mech. 69, 703–725.

Bažant, Z.P., Pang, S.D., 2007. Activation energy based extreme value statistics and size effect in brittle and quasibrittle fracture. J. Mech. Phys. Solids 55, 91–131.

Beetz, C.P., 1982. The analysis of carbon-fiber strength distributions exhibiting multiple-modes of failure. Fibre Sci. Technol. 16, 45–59.

Behzadi, S., Curtis, P.T., Jones, F.R., 2009. Improving the prediction of tensile failure in unidirectional fibre composites by introducing matrix shear yielding. Compos. Sci. Technol. 69, 2421–2427.

Beyerlein, I.J., Phoenix, S.L., 1996a. Statistics for the strength and size effects of microcomposites with four carbon fibers in epoxy resin. Compos. Sci. Technol. 56, 75–92.

Beyerlein, I.J., Phoenix, S.L., 1996b. Stress concentrations around multiple fiber breaks in an elastic matrix with local yielding or debonding using quadratic influence superposition. J. Mech. Phys. Solids 44, 1997–2039.

Carpinteri, A., 1994. Scaling laws and renormalization-groups for strength and toughness of disordered materials. Int. J. Solids Struct. 31, 291–302.

Curtin, W.A., 1991. Theory of mechanical properties of ceramic-matrix composites. J. Am. Ceram. Soc. 74, 2837–2845.

Curtin, W.A., 1993. The tough to brittle transition in brittle matrix composites. J. Phys. Mech. Solids 41, 217–245.

Curtin, W.A., 1999. Stochastic damage evolution and failure in fiber-reinforced composites. Adv. Appl. Mech. 36, 163–253.

Curtin, W.A., Takeda, N., 1998. Tensile strength of fiber-reinforced composites: I. Model and effects of local fiber geometry. J. Compos. Mater. 32, 2042–2059.

Curtis, P.S., 1986. A computer model of the tensile failure process in unidirectional fibre composites. Compos. Sci. Technol. 27, 63–86.

Daniels, H.E., 1945. The statistical theory of the strength of bundles of threads. I. Proc. R. Soc. A—Math. Phys. Eng. Sci. 183, 405–435.

Dow Plastics, 1999. Dow liquid epoxy resins. Form No. 296-00224-0199 WC+M ⟨http://epoxy.dow.com/epoxy/tech/index.htm⟩, last accessed on 29 January 2011.

Fukuda, H., Kawata, K., 1977. On the strength distribution of unidirectional fibre composites. Fibre Sci. Technol. 10, 53–63.

Gulino, R., Schwartz, P., Phoenix, S., 1991. Experiments on shear deformation, debonding and local load transfer in a model graphite/glass/epoxy microcomposite. J. Mater. Sci. 26, 6655–6672.

Harlow, D.G., Phoenix, S.L., 1978a. The chain-of-bundles probability model for the strength of fibrous materials. I: analysis and conjectures. J. Compos. Mater. 12, 195–214.

Harlow, D.G., Phoenix, S.L., 1978b. The chain-of-bundles probability model for the strength of fibrous materials. II: a numerical study of convergence. J. Compos. Mater. 12, 314–334.

Harper, L.T., Turner, T.A., Warrior, N.A., Rudd, C.D., 2007. Characterisation of random carbon fibre composites from a directed fibre preforming process: the effect of two filamentisation. Composites Part A—Appl. Sci. Manuf. 38, 755–770.

Hedgepeth, J.M., 1961. Stress Concentrations in Filamentary Structures. Technical Report TN D 882. NASA, Washington, DC, USA.

Hobbiebrunken, T., Fiedler, B., Hojo, M., Tanaka, M., 2007. Experimental determination of the true epoxy resin strength using micro-scaled specimens. Composites Part A—Appl. Sci. Manuf. 38, 814–818.

Kazanci, M., 2004. Carbon fiber reinforced microcomposites in two different epoxies. Polym. Test. 23, 747–753.

Kelly, A., Tyson, W., 1965. Tensile properties of fibre-reinforced metals: copper/tungsten and copper/molybdenum. J. Mech. Phys. Solids 13, 329–338.

Laffan, M.J., Pinho, S.T., Robinson, P., Iannucci, L., 2010. Measurement of the in situ ply fracture toughness associated with mode I fibre tensile failure in FRP. Part II: size and lay-up effects. Compos. Sci. Technol. 70, 614–621.

Landis, C.M., Beyerlein, I.J., McMeeking, R.M., 2000. Micromechanical simulation of the failure of fiber reinforced composites. J. Phys. Mech. Solids 48, 621–648.

Landis, C.M., McMeeking, R.M., 1999. A shear-lag model for a broken fiber embedded in a composite with a ductile matrix. Compos. Sci. Technol. 59, 447–457.

Mahesh, S., Phoenix, S.L., Beyerlein, I.J., 2002. Strength distributions and size effects for 2D and 3D composites with Weibull fibers in an elastic matrix. Int. J. Fract. 115, 41–85.

de Morais, A.B., 2001. Stress distribution along broken fibres in polymer-matrix composites. Compos. Sci. Technol. 61, 1571–1580.

de Morais, A.B., 2006. Prediction of the longitudinal tensile strength of polymer matrix composites. Compos. Sci. Technol. 66, 2990–2996.

Nairn, J.A., 1997. On the use of shear-lag methods for analysis of stress transfer unidirectional composites. Mech. Mater. 26, 63–80.

Nedele, M.R., Wisnom, M.R., 1994. 3-Dimensional finite-element analysis of the stress-concentration at a single-fiber break. Compos. Sci. Technol. 51, 517–524.

Newman, W.I., Gabrielov, A.M., 1991. Failure of hierarchical distributions of fiber-bundles. 1. Int. J. Fract. 50, 1–14.

Okabe, T., Takeda, N., 2001. A 3D shear-lag model considering micro-damage and statistical strength prediction of unidirectional fiber-reinforced composites. Compos. Sci. Technol. 61, 1773–1787.

Okabe, T., Takeda, N., 2002. Size effect on tensile strength of unidirectional CFRP composites—experiment and simulation. Compos. Sci. Technol. 62, 2053–2064.

Phoenix, S.L., Ibnabdeljalil, M., Hui, C.Y., 1997. Size effects in the distribution for strength of brittle matrix fibrous composites. Int. J. Solids Struct. 34, 545–568.

Phoenix, S.L., Schwartz, P., Robinson, H.H., 1988. Statistics for the strength and lifetime in creep-rupture of model carbon epoxy composites. Compos. Sci. Technol. 32, 81–120.

Phoenix, S.L., Smith, R.L., 1983. A comparison of probabilistic techniques for the strength of fibrous materials under local load-sharing among fibers. Int. J. Solids Struct. 19, 479–496.

Pimenta, S., Pinho, S.T. An analytical model for the translaminar tensile toughness of fibre composites with stochastic fractal fracture surfaces. J. Mech. Phys. Solids, submitted for publication.

Pimenta, S., Pinho, S.T., Robinson, P., Wong, K.H., Pickering, S.J., 2010. Mechanical analysis and toughening mechanisms of a multiphase recycled CFRP. Compos. Sci. Technol. 70, 1713–1725.

Pradhan, S., Hansen, A., Chakrabarti, B.K., 2010. Failure processes in elastic fiber bundles. Rev. Mod. Phys. 82, 499–555.

Scott, A.E., Mavrogordato, M., Wright, P., Sinclair, I., Spearing, S.M., 2011. In situ fibre fracture measurement in carbon–epoxy laminates using high resolution computed tomography. Compos. Sci. Technol. 71, 1471–1477.

Sihn, S., Kim, R.Y., Kawabe, K., Tsai, S.W., 2007. Experimental studies of thin-ply laminated composites. Compos. Sci. Technol. 67, 996–1008.

Stoner, E.G., Edie, D.D., Durham, S.D., 1994. An end-effect model for the single-filament tensile test. J. Mater. Sci. 29, 6561–6574.

Swolfs, Y., Gorbatikh, L., Romanov, V., Orlova, S., Lomov, S.V., Verpoest, I., 2013. Stress concentrations in an impregnated fibre bundle with random fibre packing. Compos. Sci. Technol. 74, 113–120.

Wada, A., Fukuda, H., 1999. Approximate upper and lower bounds for the strength of unidirectional composites. Compos. Sci. Technol. 59, 89–95.

Weibull, G.W., 1951. A statistical distribution function of wide applicability. J. Appl. Math., 293–297.

Wisnom, M.R., 1999. Size effects in the testing of fibre-composite materials. Compos. Sci. Technol. 59, 1937–1957.

Wisnom, M.R., Green, D., 1995. Tensile failure due to interaction between fibre breaks. Composites 26, 499–508.

Wisnom, M.R., Hallett, S.R., Soutis, C., 2010. Scaling effects in notched composites. J. Compos. Mater. 44, 195–210.

Zhandarov, S., Pisanova, E., Lauke, B., 1998. Is there any contradiction between the stress and energy failure criteria in micromechanical tests? Part I. Crack initiation: Stress-controlled or energy-controlled? Compos Interfaces 5, 387–404.